Flutter Prediction of Metallic and Composite Wings Using Coupled DSM-CFD Models in Transonic Flow

Hassan Ibrahim Kassem

Doctor of Philosophy

Department of Mechanical Engineering & Aeronautics

School of Mathematics, Computer Science & Engineering

December 2017

Contents

List of Figures

Figure number and caption **Page No.**

List of Tables

Table number and caption **Page No.**

Acknowledgements

First I would like to express my most sincere gratitude to my supervisor, Prof. J. R. Banerjee for his continuous help and support during my Ph.D. project. I learned a lot from him which have been reflected in this work. He is a wise mentor who is sharing his life experience and expertise with an open heart. I cannot find words to thank him for his help, support and understanding. Also, I would like to thank Dr. Xiang Liu for his support and the hours of fruitful discussions.

This project would not be even possible without the encouragement and support of my wife Ingy. We started our journey together and my Ph.D. almost at the same time. She was very supportive and patient during this journey. I will do my best to the rest of my life to pay her back for all of her sacrifices during this tough period of our journey together. I would like to thank my family, without their support I would not have even started my postgraduate studies. They were always unconditionally supportive, believing in me even at the moments of self-doubts. One important person which supported me a lot during this project is Ms. Linda Vennard. She is a wonderful friend who helped us in every step of our stay in the UK.

I want to express my gratitude and recognition to all those anonymous persons around the world who generously share their knowledge, giving their time and effort to the OpenFOAM community without expecting any reward.

Declaration

I declare that this thesis was composed by myself, that the work contained herein is my own except where explicitly stated otherwise in the text, and that this work has not been submitted for any other degree or processional qualification except as specified. Some parts of this work have been published in [1–5].

Abstract

Although flutter analysis is a relatively old problem in aviation, it is still challenging, particularly with the advent of composite materials and requirements for high-speed light airframes. The main challenge for this problem is at the transonic flow region. The transonic flow, being non-linear, poses a great challenge over traditional linear theories which fail to predict the aerodynamic properties accurately. Aerospace has been one of the primary areas of applications to take advantage of composite materials with the aim to reduce the total mass and improve control effectiveness.

This work takes advantage of CFD methods advancement as the main flow solver for non-linear governing equations. In order to investigate the dynamic behaviour of composite aircraft wings, the dynamic stiffness method (DSM) for bending-torsion composite beam is used to compute the free vibration natural modes. The main objective of this work is coupling the dynamic stiffness method (DSM) with high fidelity computational fluid dynamics models in order to predict the transonic flutter of composite aircraft wings accurately and efficiently. In addressing the main aim of this study, Euler fluid flow solvers of an open source CFD code called OpenFOAM has been coupled with elastic composite wing, represented by the free vibration modes computed by DSM.

The first part of this study is devoted to investigating the free vibration characteristics of two types of aircraft, namely sailplane type and transport airliner type. Two models of each type have been analysed and contrasted, which revealed the significance of the natural modes of aircraft wings and how these modes inherently capture the essential characteristics of the system. Then to validate the CFD code, two pitching and self-sustained two degrees of freedom airfoils under different flow condition have been modelled. The results have been compared against experimental measurements and numerical data from the literature which showed good agreement for the predicted force coefficients. Finally, the model has been extended to study a complete aircraft wing. Both metallic and composite Goland wings have been investigated under a wide range of flow conditions. The composite wing has been investigated using different material coupling values to show their effect on its aeroelastic behaviour. The results showed the significant influence of the material coupling on the aeroelastic characteristics of composite wings.

Chapter 1

Introduction

1.1 Motivation

Composites are made of wide range of materials which have different properties. For laminated composites, these are one main continuous phase (matrix) and one discrete phase (filments, fibers) [6] . Composites in general can be traced back to prehistoric days, and they have been available in nature as well, for example wood. The first man-made composites appear to be recorded on the walls of the ancient Egyptian's templates as a corner stone of the building procedure. A mixture of straw and mud is still used in some parts of the world as buliding material which is a clear example of composites. Even the concept of present day laminated composites were known to the ancient Egyptians particularly in the form of plywood [7, 8].

The usage of composites paved the way to human controlled materials. These materials are distinguished from the metal alloys in many aspects. The main difference is in anisotropy which means that the material properties for

composites change with direction, specifically the strength and the stiffness. The advent of composites opened new horizons in many engineering applications. Aerospace has been one of the primary areas of applications to take advantage of composite materials.

The main benefits of using composites particularly in the aviation industry are the high specific strength and directional properties of composites. The low density of composites is translated directly into weight reduction which is a major consideration in aircraft design. In essence, the first step towards a conceptual design after specifying the mission profile is to estimate the initial weight [9]. The reduced weight means increased range, less fuel consumption and higher pay load. Additionally, composites can improve the aerodynamic performance due to their smooth finish over the wing and the airframe.

Despite the superior flexibility in optimizing the characteristics of composite materials compared to metallic alloys of Aluminium (which are widely used in aerospace applications) the usage of composites did not grow as much as anticipated [10]. Some of the reasons behind this were the cost of production, adapting new manufacturing techniques and obtaining the required certifications for the new component. Also, the low strength through the thickness of laminates and the low resistance to mechanical failure are some of the contributing factors which prevented the expansion in the usage of composites. An important fact should be mentioned and stressed upon is that the usage of composite is nevertheless increasing and the above disadvantages of composites are only the reasons behind not rapid expansion of usage and not meeting the expectations as anticipated. The Boeing 787 development of dreamliner and

Airbus A350 are very good examples, which overcame the problem showing extensive usage of composites.

Many of the concerns of using composite materials have been tackled in the past decade, which made advanced composite material a very important candidate in many of the applications today. It is expected that the trend of growth in using composites will continue not only because of the advantages of composites or because of overcoming many of the disadvantages but also because of the decrease in the cost of production. It is anticipated that the concerns about the climate change and the expected new rules will encourage the usage of composites further more in future. Today, a glimpse of this future can be seen from the historical development of the solar impulse aircraft [11, 12]. Composite materials are the main materials used in this type of aircraft and there is no doubt that any metallic alloy aircraft cannot compete in this category. The attachment of the solar panels over the aircraft wing could indeed be considered as a composite structure.

In addition to the engineering and manufacturing challenges faced by the usage of composites, theoretical questions and challenges also arose very considerably. The first and the foremost fundamental question was how to predict the properties of such new materials theoretically and experimentally. Moreover, an important question was how to optimise the material properties for specific application by taking advantage of the anisotropic nature of fibrous composites. Obviously, this added new dimensions and complexity to the design process. One of the main areas of interest in the aerospace applications is the aeroelastic behaviour of composite structures.

It was not surprising that aeroelasticity captured the main attention because of its essential role in aircraft design. Inaccurate predication of the aeroelastic characteristics of aircraft during the design process can lead to catastrophic incidents. One of the most dangerous aeroelastic instabilities is of course, flutter. It is a self-excited oscillation of elastic body in fluid stream. Flutter speed defines the speed beyond which the aircraft becomes unstable [13–15]. It means that if the aircraft flies at this speed it will have steady harmonic oscillation of constant amplitude. This point is the most critical point which gives flutter speed because if for any reason, the free stream velocity exceeds this speed, the system will have divergent oscillation and will eventually vibrate in a violent manner which could lead to the destruction of the aircraft.

The complexity of flutter analysis arises from the fact that flutter involves very strong coupling between fluid mechanics and structural dynamics. Therefore, an accurate description of the flow field as well as structural dynamic behaviour together with a mechanism of coupling them is essential for flutter analysis. Avoiding flutter is a mandatory requirement in any aircraft design process. Although flutter analysis is a relatively old problem in aviation, but it is still challenging, particularly with the advent of composite materials and the requirements of high speeds and light airframes. The structural dynamics is an essential part of this problem which could be tackled using different theories and methods. In this work, the dynamic stiffness method (DSM) for bending-torsion coupled beam elements is used to compute the free vibration natural modes of high aspect ratio aircraft wings.

The dynamic stiffness method is an analytical method which solves in an

exact sense the governing equations of a structural system. In some respects, it is comparable with the finite element method (FEM). However, the FEM is an approximate numerical method in which the accuracy of the solution depends on the number of the elements used in the analysis and the assumed shape function. On the other hand, the DSM is independent of the number of elements used in the analysis. For instance in the case of a uniform aircraft wing, the free vibration problem can be solved by using only one element without compromising the accuracy [16].

The main challenge in this thesis is to solve the aeroelastic problem in the transonic flow region. The transonic flutter limit appears to be low in any flight range. Therefore, for an aircraft the most critical flutter point generally arises when the flow is transonic. The phenomenon is called transonic dip which has been featured in the literature many times [17–19]. The transonic flow field is a transition between subsonic flow and supersonic flow exhibiting shock waves and highly non-linear behaviour.

The transonic flow being highly non-linear poses a formidable challenge over traditional linear theories [19] which fail to predict the aerodynamic properties accurately. Therefore, solving the non-linear governing equations of fluid flow using numerical techniques has become essential [15, 20–22], particularly when solving aeroelastic problems. Despite the computational cost of using computational fluid dynamics (CFD), it is necessarily being used in the aeroelasticity field for greater accuracy and better flutter prediction. This has given birth to a relatively new field in aeroelasticity called computational aeroelasticity [23, 24] which couples CFD with CSD (computational structural dynamics).

1.2 Problem Statement

This research is aimed to predict accurately the transonic flutter by using the finite volume method when solving the flow field non-linear governing equations in a closely coupled way together with the dynamic stiffness method (DSM) as the structural model. Then an integrated methodology is used to predict the transonic flutter of composite wings. In order to achieve this objective the following systematic research steps are followed:

- To develop and make the best use of OpenFOAM (Open source CFD code) as the main CFD solver.
- To model two-dimensional unsteady flow over forced pitching and heaving aerofoils and validate the current solvers and to implement additional tools in OpenFOAM when required.
- To implement new boundary conditions in OpenFOAM in order to compute the aerofoil displacement based on free vibration natural modes.
- To extend the work to three-dimensional aircraft wings and validate the results for metallic wings.
- To couple the CFD solver with the free vibration natural modes from the dynamic stiffness method for composite wings.
- To carry out parametric study by changing the significant parameters of composite wings.

1.3 Thesis Map

This introduction chapter is followed by Chapter 2 which is basically a literature review chapter on transonic flutter analysis. Then Chapter 3 describes the mathematical formulation and modelling techniques used in this study. The next three chapters present the results and discussion for different cases. In particular Chapter 4 highlight the free vibration characteristics of sailplanes and transport airliners wings. In Chapter 5, the aerodynamic model is considered in detail and extensively validated. Moreover, the fluid-structure interaction is incorporated in this chapter to model the elastic behaviour of the structure. Chapter 5 also focuses on typical wing sections (aerofoils). By contrast Chapter 6 focuses on a complete cantilever wings. In particular, Goland wing which is extensively reported in the literature is considered. Two versions are investigated, namely metallic and composite versions. Finally, general conclusions and future recommendations are discussed in Chapter 7. The appendices give brief description of the newly developed code for this work.

Chapter 2

Literature Review

2.1 Computational Aeroelasticity

In 1998, Guruswamy [25] investigated the influence of high performance parallel computing on aeroelasticity field. He showed how the multidisciplinary field of computational aeroelasticity emerged and enhanced due to the availability of this new computational power, which allowed tackling the coupled problem using high fidelity models. He predicted that CFD/CSD models will play a larger rule in the future which has become a reality today.

By contrast, Bennett et al. [20] argued that computational aeroelasticity overall was too expensive to solve stability problems such as flutter. The authors argued that, it would be computationally more efficient to use such high fidelity models in cases where linear theories were well known for their limitation. Also, they stated that computational aeroelasticity would be impractical without innovative solution techniques and implementation methods.

Without doubt, the multi-physics computational problems in general are

more affordable today than before, but some problems such as flutter are still computationally expensive in this respect. Specially, in the early stages of design it is nevertheless needed for certain cases such as establishing the transonic flutter. Therefore, it is expected that both high fidelity and low fidelity models will stay as an efficient comparable solution. It is up to the design engineer to select the tools which are most efficient and suitable for the job in hand. In this work, the dynamic stiffness method (DSM) is used to compute the free vibration modes which are subsequently used as input for the CFD Euler model. The structure model using DSM is exact but because only the mode shapes represented a limited number of degrees of freedom, it is considered to be a low fidelity model. The aerodynamic model on the other hand is reduced from Navier-Stokes to Euler system (inviscid flow) as described in Chapter 3 which is still considered to be a high fidelity model.

2.2 Aerodynamics

The study of the aeroelastic behaviour poses many aerodynamical challenges. The first major problem is to deal with the flow unsteadiness which is essential to predict an aeroelastic phenomenon like flutter. Therefore, unsteady aerodynamics has been a major area of interest in the aeroelastic community. An important breakthrough which made aeroelastic analysis possible was Theodorsen's theory for oscillatory aerofoils [26]. Theodorsen's theory is valid only for unsteady incompressible flow which can be considered to be the first practical solution for this type of flow, as descried by Blair [27].

In addition to the flow unsteadiness that are prevalent in many aeroelastic studies, another major challenge faced by researchers is the problem arising from flow non-linearity. As mentioned in Chapter 1, when the aircraft speed becomes faster and the normal cruise speed becomes near the sonic-speed (transonic speed), it is essential to predict the non-linear flow accurately. Bendiksen discussed the importance of predicting this non-linear behaviour and the underling reasons for this in his review article [19].

Transonic flow is essentially a mixture of subsonic and supersonic flow with some complicated interactions. The flow usually get accelerated around the wing which converts the free stream subsonic flow into supersonic flow. This supersonic flow creates normal shock waves which sharply reduces the flow speed to subsonic. This gives rise to some kind of supersonic pockets over the wing and because the wing is an elastic structure, its deformation oscillates the flow around it. As a consequence this leads to oscillating shock waves and oscillating flow in general. Therefore,, this combination of oscillating flow regions are indeed spatially and temporally non-linear. Moreover, the discontinuity due to the presence of shock waves increases the flow non-linearity.

Another source of non-linearity is due to the wing shape which leads to complex flow behaviour such as wakes, turbulence and flow separation. Thus, in order to accurately predict the transonic flutter, non-linear unsteady aerodynamic theories are essential. These theories should be able to predict the shock waves and their location. Also, it should be able to predict the different flow regions as a part of the solution.

For the above mentioned reasons computational fluid dynamics (CFD) be-

came a major player in the area of computational aeroelasticity over the last three decades. This trend is expected to grow in the future and CFD will be the main aerodynamic tool specially when dealing with transonic flow [28].

2.2.1 Linear Potential Flow

Under the assumptions that the flow is incompressible, inviscid (no viscosity) and irrotational, flow velocity field can be described by means of scalar field velocity potential [29]. Incompressibility assumes that the change in the flow density ρ is small or more precisely relatively small. Therefore, the density changes can be ignored which can be represented mathematically as divergence free velocity field.

It is intuitive to understand the implications of the inviscid assumption which means ignoring the viscous forces entirely. This means there is no shear between the flow layers and indeed there is no appreciable turbulence. However, the consequences of the irrotational assumption may not be so clear at first sight. Imagine a very small flow element moving along a certain path. If this element is translating without rotation and maintains its original shape, this flow is called irrotational flow.

Under the above assumption that the velocity field can be represented by the gradient of a scalar field $\mathbf{U} = \nabla\phi$, where (ϕ) is the velocity potential is represented by a second order linear partial differential equation (Laplace's equation). This linear behaviour indicates that the sum of any number of particular solutions ϕ is also a solution [30].

2.2.2 Transonic Small Disturbance Theory

The main assumptions for transonic small disturbance theory as pointed out by Cole [31] are that the flow is inviscid and the fluid is a perfect gas. Indeed such assumptions are valid for certain transonic flow situations. However, in many ways these restrictions are the same as those of Euler equations. The difference is that the theory assumes a small disturbance in flow field compared to a uniform state which means it is valid only for thin bodies. Although the theory originally considered steady flow only and thus problems such as flutter were not considered, nevertheless, it introduced a key feature, namely non-linearity to many engineering tools [19, 31–33]. The theory is able to predict mixed regions of subsonic and supersonic regions.

Later, the transonic small disturbance has been extended to include the unsteady flow and one of the early formulation was introduced by Ballhaus et al. [34]. The authors validated the theory for flow over swept wing and compared the results for subcritical and supercritical Mach numbers. The results generally showed good agreement with experiment and results using panel techniques. However, the investigation showed a larger difference in the subcritical region, which could be attributed to the treatment of the compressibility and because of not considering the viscous effect.

The viscosity was included afterwards by other researchers [35, 36]. This method was implemented in one of NASA well-known codes CAP-TSD [37] for inviscid aeroelastic applications. Another version of this code (CAP-TSDV) for viscous flow was released afterwards. In this version the flow is solved for two regions, one is viscous (boundary layer) and the other one is inviscid

[38–40]. However, this method did not predict the very low supersonic Mach number accurately.

2.2.3 Euler Equations

In many cases where there is no flow separation and the viscous effect does not dominate the flow field, Euler model is very effective and can be an accurate model. For high speed transonic and supersonic flow (high Reynolds number cases), the inertia force is much larger than the viscous force and dominates the flow physics. Ignoring the viscosity reduces the momentum equation to Euler equation which could be solved with continuity and energy conservation equations to predict the flow field. Additionally, the equation of state is solved to relate the pressure to density and temperature.

Hence, the only assumption here is that the flow is frictionless. As a consequence, it makes Euler model a very good candidate for aeroelastic analysis. But, it is more expensive than the small-disturbance model which somehow made the Euler code computationally expensive for flutter analysis in early seventies. Magnus and Yoshihara [41] introduced the steady model for flow over aerofoils using Euler code. They showed some promising result despite some discrepancies around the shock waves. Later the same authors developed an unsteady finite difference solver for flow over aerofoils [42]. A decade later, Jameson et al. [43] modelled inviscid transonic flow over an entire aircraft. The authors showed promising preliminary results, using a novel meshing technique and multi-grid acceleration method.

In the late 1980's NASA developed ENS3DAE code for Euler/Navier-Stokes

for aeroelastic applications [44]. This code subsequently evolved and extensively validated. In this respect, Smith et al. [45] were the earliest investigators to do so. In their work they validated the code for both steady and unsteady flow over NACA 64A-006 aerofoil and F-5 wing. Schuster et al. [46] reported two case studies, namely Goland wing (heavy version [47]) and BACT wing [48]. The main purpose was to validate the new deforming mesh capabilities in ENS3DAE. Lewis and Smith extended the model to predict the shell flutter [49], which revealed interesting results.

2.2.4 Navier-Stokes Equations

Like Euler equations model, Navier-Stokes equations model solves a system of nonlinear equations. The main difference is that the viscous effect is not ignored in Navier-Stokes equations which has important implications leading to computationally expensive model for aeroelastic problems. The first point which must be addressed is the variation in dynamic viscosity due to the aerodynamic heating, which means extra formula is needed to calculate the viscosity such as Sutherland's law [50].

However, the expensive part is due to solving the boundary layer and the turbulence. In order to solve the boundary layer a very small grid cells near the wing surface are required. This means that more computational points and smaller time step are required to maintain numerically stable solution. Moreover, because this is generally not possible (computationally, $N_{cells}\,\alpha\,Re^{9/4}$) to solve Navier-Stokes equations directly for high Reynolds number flows (DNS) turbulence models are essentially needed. In principle, the system can be

solved for averaged parameters which results a closure problem for stress tensor. There are many strategies to solve this problem in CFD which require solving extra governing equations for turbulence and put more constraints on the meshing and time step [51–53].

Although the computational cost is high, this model is still used for flutter predication but not as widely as the previous models. It is part of ENS3DAE code [45] and CFL3DAE which is an extension for NASA CFL3D CFD code [54, 55]. Lee-Rausch and Baitina [54] compared Euler and Navier-Stokes models in flow predications for ARGAD Wing 445.6 swept wing. The results were within 2% of the experimental measurements, but both models predicted almost the exact flutter boundary over wide a range of Mach numbers. It is worth mentioning here that for specific cases and conditions, the viscous effect may have a significant impact as reviewed by Bennett and Edwards [20].

Another interesting study by Bartels and Schuster [56] compared the two codes, ENS3DAE and CFL3DAE. Despite the many differences between the codes in implementation of dynamic mesh treatment and turbulence models, they showed very good agreement in predicting flutter boundary of BACT wing. Huttsell et al. [57] evaluated and highlighted the main differences between aeroelasticity codes. Higher fidelity turbulence models such as large eddy simulations (LES) are still unaffordable for aeroelastic applications in general [19, 58].

2.3 Dynamics Stiffness Method

As described very briefly in Chapter 1, the dynamic stiffness method (DSM) is an eigenvalue solving technique to compute the free vibration frequencies and mode shapes of structures. In sharp contrast to the finite element method (FEM), DSM is an exact method. DSM was originally developed by Koloušek in the 1940s [59, 60] when he introduced the concept of frequency dependent dynamic stiffness matrix. The main advantages of the DSM compared to FEM can be examined by understanding the fundamental key concepts of both theories.

The core concept in FEM is to represent the system by two matrices, namely the mass and stiffness matrices. These matrices represent the nodal (point) equivalent mass and stiffness properties which relate the system displacement and forces. The mass and stiffness matrices can then be reformulated leading to linear eigen value problem from which the natural modes of the system can be calculated. The method inherently approximates the relation between nodal displacement and element deformation by using the so called shape function [16]. This function is usually assumed as polynomial functions in terms of some arbitrary constants. Although the method is efficient, it implicitly includes a certain degree of approximation. Furthermore, the total number of modes which can be computed are limited by the number of elements, and thus in order to obtain a higher number of frequencies, more elements are required. Clearly this is translated into higher computational cost and less accuracy.

In DSM there is no assumed shape function as such because the deformed shape is obtained directly from the governing equations of motion under free vibration conditions. Therefore, the resulting dynamic stiffness matrix is frequency dependent. In order to compute the free vibration modes, a non-linear eigen value problem must be solved in DSM. The main solving techniqe for this problem is the Wittrick-Williams algorithm [61, 62]. The Wittrick-Williams algorithm is capable of obtaining all natural frequencies up to any desired accuracy, independent of the number of elements (size of the matrix) used in the analysis. Although solving the non-linear eigen value problem in general is more expensive than solving the linear problem, the DSM is more efficient because less element can be used to obtain the same number of frequencies. Even only one element can be used to obtain any number of frequencies accurately. It is worth mentioning here that there are no approximations or assumptions made to drive the dynamic stiffness matrix from the differential governing equations of motion, which makes the method exact in this sense. An in-depth review about DSM in general and its historical development can be found in [16].

2.3.1 Beam Element Representation

Beam is one of the fundamental elements in many engineering applications. One of the earliest applications of DSM using beams was demonstrated by Williams and Wittrick [63]. This work considered only pure bending of isotropic beams (Bernoulli-Euler). Shortly after, more accurate method was developed for axially loaded isotropic Timoshenko beams [64, 65]. At this point the

theory gained a lot of attention and implemented in many software packages [66, 67]. However, one software in particular has most up to date feature at the time is BUNVIS-RG [68] which used exact matrices for Bernoulli-Euler isotropic uniform and tapered beams [69, 70].

In the recent phase of its development the method made its way to aeroelasticity research with the extensive development of the DSM for bending-torsion coupled beams [71, 72]. By the late 1980's and early 1990's, the method was generalised and implemented in a new software developed by Banerjee [73, 74]. This step was significant because in many engineering applications, there is always a shift between the mass axis and the elastic axis such as that of an aircraft wing. Banerjee et al. continued developing the method to include twisted Timoshenko beam [75] , spinning beams [76]. Later, Pagani et al. [77] used Carrera Unified Formulation to incorporate the cross-sectional deformation of the beam.

As composite materials entered many engineering applications specially aerospace industry, the need for DSM formulation for composite beams became clear. In 1995, Banerjee and Williams [78] introduced DSM formulation using symbolic computing . These new explicit algebraic expressions showed significant reduction in computational time compared to matrix inversion methods. This work was based on bending-torsion beam theory and incorporated extra terms to include the materiel coupling in composite materials. As for isotropic materials, DSM has been developed for different type of beams such as axially loaded Timoshenko beams [79] and section shear deformation theory [80]. A very import concluding step was achieved by combining both material coupling

and geometrical coupling to compute the free vibration modes of aircraft wings which shows the significance of DSM in real engineering applications [81].

2.4 Coupling Fluid and Structure Models

Due to the variety of fluid and structure models, a diverse range of coupling techniques were developed in the past [22]. Each code has its coupling strategy based on the implemented models [82, 83]. Domain decomposition is normally used to allow solving the structure and fluid with different suitable solvers as opposed to solving both as one system. Both domains could be solved independently (sequentially) by obtaining the aerodynamic forces first then applied to the structure. In this method, there is no feedback from the structure solver to the fluid solver. Guruswamy and Yang [84] used this approach to study the pitch-heave response of thin NACA 64A006 aerofoil in transonic flow. This approach is limited to the cases where the structure system is much stiffer than the flow system. Therefore, closely coupled strategies are the norm nowadays because of their numeric efficiency and accuracy [22].

In coupled models, the aerodynamic forces are calculated first and within the same time step they are transferred to the structure solver. Then the displacements are computed and transferred back to the fluid solver. In this approach an interface mesh is used to interpolate the forces and displacements between the two solvers. The interfacing method depends mainly on the used models on both sides. For example, in case of modal analysis the structure is represented by a grid of nodes, for beam just one dimensional grid. The forces

are integrated over the wing surface and interpolated into the modal grid [82]. Once the displacements of the modal grid are computed, the wing is deformed based on that. This approach is used in this work, see Chapter 3.

Chapter 3

Theoretical Background and Problem Formulation

This chapter describes the problem in mathematical terms. The main aspects of modelling the fluid-structure interaction problem are covered starting from the aerodynamic and structural considerations with particular emphasis on the coupling between them. Furthermore, the modelling challenges and their possible solutions are discussed and the proposed methodologies in this research are highlighted.

3.1 Aerodynamic Model

3.1.1 Governing Equations

The governing equations of the flow used in this work are those of the complete Euler equations [85–87]. The only assumption at this level in Euler equations compared to Navier-Stokes equations is the assumption that the viscous forces

are considered negligible. This assumption is considered legitimate and applicable to many aerospace problems where the flow velocity is relatively high and the influence of the boundary layer is relatively small [29]. If ρ, $\mathbf{U}$, p and E are density, velocity, pressure and total energy respectively, the Euler equations in vector notation have the following used form:

- Conservation of mass:

$$\frac{\partial \rho}{\partial t} + \nabla \cdot [\mathbf{U}\rho] = 0 \tag{3.1}$$

- Conservation of momentum:

$$\frac{\partial (\rho \mathbf{U})}{\partial t} + \nabla \cdot [\mathbf{U}(\rho \mathbf{U})] + \nabla p = 0 \tag{3.2}$$

- Conservation of total energy:

$$\frac{\partial (\rho E)}{\partial t} + \nabla \cdot [\mathbf{U}(\rho E)] + \nabla \cdot [\mathbf{U}p] = 0 \tag{3.3}$$

where ∇ denotes the nabla vector operator given by , $\nabla \equiv \partial_i \equiv \frac{\partial}{\partial x_i} \equiv (\frac{\partial}{\partial x_1}, \frac{\partial}{\partial x_2}, \frac{\partial}{\partial x_3})$. Thus for any vector $\mathbf{a}$, $\nabla \cdot \mathbf{a}$ is the divergence defined by $\nabla \cdot \mathbf{a} \equiv \frac{\partial a_1}{\partial x_1} + \frac{\partial a_2}{\partial x_2} + \frac{\partial a_3}{\partial x_3}$ where a_1, a_2 and a_3 are the components of a in x_1, x_2 and x_3 direction respectively. Also for any scalar s, the gradient is $\nabla s \equiv (\frac{\partial s}{\partial x_1}, \frac{\partial s}{\partial x_2}, \frac{\partial s}{\partial x_3})$. In equation (3.3), the total energy $E = e + \frac{|\mathbf{u}|^2}{2}$ with e the specific internal energy.

3.1.2 The Fluid Solver

The main purpose of this work is to predict the transonic flutter. In this regime the flow is highly non-linear and unsteady. Moving and oscillating shock waves are the dominant features of transonic flow field. In order to predict such complex flow field with high fidelity model, a special technique needs to be applied to solve the governing equations outlined in section 3.1.1. In general there are two main approaches to solve the above equations (3.1)-(3.3) using CFD. These are essentially either pressure based solver or density based solver. The main difference between them is that the latter solves the continuity equation as a function of density, directly coupled with the rest of governing equations. This is in contrast to the pressure based solver which solves a pressure correction equation which is derived from the momentum and continuity equations [86]. This pressure correction works as a constraint on the velocity field to satisfy the continuity equation.

Both approaches are available in OpenFOAM for high speed compressible unsteady flow. In OpenFOAM, the pressure based solver is called `sonicFoam` and the density based solver called is `rhoCenteralFoam`. The advantages and disadvantages of each method are well known amongst the CFD community [85, 86]. The main advantage for pressure based solver is that it requires less computational resources than the density based solver due to the segregation between the governing equations. The obvious advantage of density based solver is the coupling between the governing equations which leads to better non-oscillating solution, specially when discontinuities are involved due to shock waves. In this work both solvers have been used and they did not

show major differences with respect to flutter predictions. The implementation of `rhoCentralFoam` reveals some of the advantages of Riemann solver [87]. A full comparison between the implementation of the two methods in OpenFOAM showed better results of `rhoCentralFoam` solver over sonicFoam in different high speed compressible flow cases [88]. The density based solver, `rhoCentralFoam` uses central difference schemes based on Kurganov and Tadmor formulation introduced in 2000 [89]. It was implemented in OpenFOAM by Greenshields et al. in 2009 [87]. It is a semi-discrete, non-staggered central scheme. The `sonicFoam` solver is based on PIMPLE algorithm which is fully described in [88].

3.1.3 Dynamic Mesh Modelling

Solving a particular fluid-structure interaction problem involves a moving solid object requiring some special strategy to include the movement. In this respect, finite volume method is generally used for solving fluid dynamics governing equations at fixed cells in space (control volumes) around the geometry. When the solid objects start to move there will be a relative velocity between the boundaries and the mesh cells. There are two usual approaches to solve this problem. The first approach relies on calculating the movement of the mesh according to its boundary displacement but maintaining the same number of grid cells. The second approach is to calculate the new position of each grid cell with the possibility of removing or adding new cells as required. These two techniques already implemented in OpenFOAM are particularly useful [90, 91].

In this study, the first approach mentioned above is used which basically solves Laplace equation for the grid displacement at every time step [90–92]. A diffusion coefficient for the mesh movement is essentially the only parameter important that should be specified by the user. Before describing the governing equation of moving grid, it is useful to examine the main differences between static and dynamic mesh. Basically it is the relative speed between the boundary and the mesh which has a direct relation with the flux through each finite volume cell. Ignoring this relative speed could lead to numerical error in the solution. Preventing this numerical problem requires applying the space conservation law (SCL) which states [85, 90]

$$\frac{d}{dt}\int_V dV - \oint_S n \cdot v_s dS = 0 \tag{3.4}$$

where V is an arbitrary moving volume, n is the unit vector normal to the surface and v_s is the surface speed. The above condition applied in OpenFOAM solvers by a function called `makeRelative`. In OpenFOAM the name of the solvers which are capable of handling dynamic meshes includes `"DyM"`. For example the variants of `rhoCentralFoam` and `sonicFoam` solvers which are used in this study for dynamic mesh are `rhoCentralDyMFoam` and `sonicDyMFoam` respectively. Now attention is turned to the Laplace displacement mesh motion solver in OpenFOAM, which solves for independent displacement vector $\mathbf{d}$ defined by

$$\mathbf{r}(t + \Delta t) = \mathbf{r}(t) + \mathbf{d} \tag{3.5}$$

where $\mathbf{r}$ is the point position vector. Thus, Laplace equation for mesh motions

with k as diffusion coefficient is

$$\nabla \cdot (k \nabla \mathbf{d}) = 0 \tag{3.6}$$

Equations (3.4) and (3.6) illustrate the main difference between static mesh solvers and dynamic mesh solvers in OpenFOAM.

3.1.4 Wing Boundary Condition

A special boundary condition for moving walls velocity associated with dynamic mesh solver is required to satisfy space conservation law. For viscous flow, such boundary condition is called `movingWallVelocity` which makes the normal flux to the wall equal to zero. A variant of this boundary condition was developed for this study which ensures that the tangential velocity on the wall is equal to the flow tangential velocity at the contact point. Lewis and Smith [49] used a very similar boundary condition for flutter prediction using the ENS3DAE solver [45]. In other words it is a slip wall boundary condition for moving walls because the flow considered inviscid as described in section 3.1.1. This boundary condition has been adapted and implemented in OpenFOAM for this work.

3.1.5 Non-reflecting Outlet Boundary Condition

The compressible high speed flow is dominated by pressure wave which propagate with the sound in the flow field. These waves are responsible of transforming the information between the fluid particles, thus when the flow speed

reaches the sonic speed, shock waves start to appear [29]. Therefore, a special outlet boundary condition is required to eliminate any pressure wave reflection. This boundary condition allows the wave to go out of the computational domain without reflecting back inside the domain.

In this investigation a boundary condition called `waveTransmissive` has been used which serve this purpose. It could be classified as non-reflective advective boundary condition which is applied locally according to Givoli's definition [93]. This boundary condition is based on solving equation (3.7) on the boundary field Φ.

$$\frac{D(w\Phi)}{Dt} = 0 \tag{3.7}$$

In equation (3.7), D/Dt is the total derivative and w is the total wave speed at the boundary which is calculated as,

$$w = \frac{\phi}{S_f} + \sqrt{\frac{\gamma}{\beta}} \tag{3.8}$$

where ϕ is the face flux, S_f is the face area of the boundary, γ is the specific heats ratio which equals to 1.4 for ideal gas and β is the flow compressibility at the boundary. The first term in equation (3.8) represents the flow normal velocity to the boundary and the second term is basically the local speed of sound. Using this boundary conditions corrects the pressure value at the outlet boundary to ensure no wave reflection.

3.2 Structure Model

3.2.1 Typical Wing Section

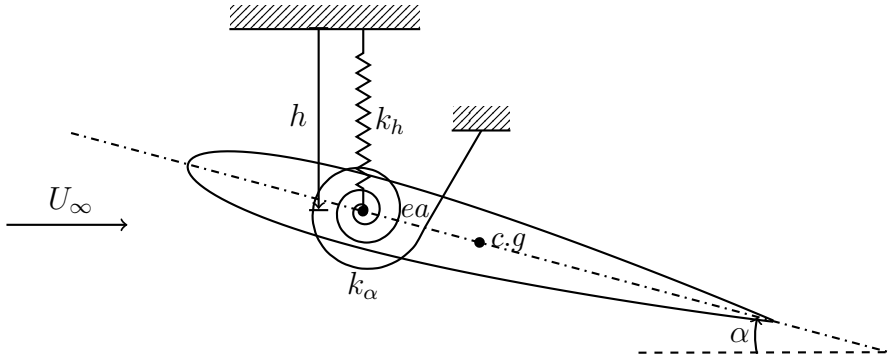

Figure 3.1: Typical wing section

The typical wing section using two-dimensional model [13, 15, 94] is well established for studying two degrees of freedom flutter. This model considers the plunging (h) and pitching (α) motions about the elastic axis of the wing. The governing differential equations of undamped motion are [95]:

$$m\ddot{h} + S_\alpha \ddot{\alpha} + K_h h = -L \tag{3.9}$$

$$S_\alpha \ddot{h} + I_\alpha \ddot{\alpha} + K_\alpha \alpha = M_{ea} \tag{3.10}$$

where m, I_α and S_α are aerofoil mass per unit length, section moment of inertia about the elastic axis per unit length and static mass imbalance respectively. In equations (3.9) and (3.10), K_h and K_α are bending and torsional spring stiffness whereas L and M_{ea} are the lift force (positive up) and pitching moment about the elastic axis (positive nose up). The plunging displacement h is positive down and the angle of attack α is positive nose up and is in radians. Non-dimensionalizing the linear displacement by the aerofoil semichord (b) in

equations (3.9)-(3.10) and the time by the uncoupled natural frequency of the torsional spring (ω_α) so that the dimensionless time is $\tau = \omega_\alpha t$. The governing equations (3.9) and (3.10) can now be rewritten in the following matrix form

$$[M]\{\ddot{q}\} + [K]\{q\} = \{F\} \tag{3.11}$$

where

$$[M] = \begin{bmatrix} 1 & x_\alpha \\ x_\alpha & r_\alpha^2 \end{bmatrix} \qquad \{F\} = \frac{U_\infty^2}{\pi\mu\omega_\alpha^2 b^2} \begin{Bmatrix} -C_l \\ C_m \end{Bmatrix}$$

$$[K] = \begin{bmatrix} (\frac{\omega_h}{\omega_\alpha})^2 & 0 \\ 0 & r_\alpha^2 \end{bmatrix} \qquad \{q\} = \begin{Bmatrix} \frac{h}{b} \\ \alpha \end{Bmatrix}$$

In equation (3.11), $[M]$ and $[K]$ are the mass and stiffness matrices, and $\{F\}$ and $\{q\}$ are the force and displacement vectors. The non-dimensional aerofoil mass ratio is $\mu = \frac{m}{\pi\rho b^2}$ with x_α and r_α being the static unbalance and the radius of gyration respectively. The uncoupled natural frequencies in plunging and pitching motion are ω_h and ω_α, respectively. C_l and C_m represent the lift and pitching moment coefficients which have the same sign convention as the aerodynamic forces and moment L and $M_e a$. The forces coefficients are defined as

$$C_l = \frac{L}{\frac{1}{2}\rho U_\infty^2} \tag{3.12}$$

$$C_M = \frac{M_e a}{\frac{1}{2}\rho U_\infty^2 c} \tag{3.13}$$

3.2.2 Beam Element Idealisation

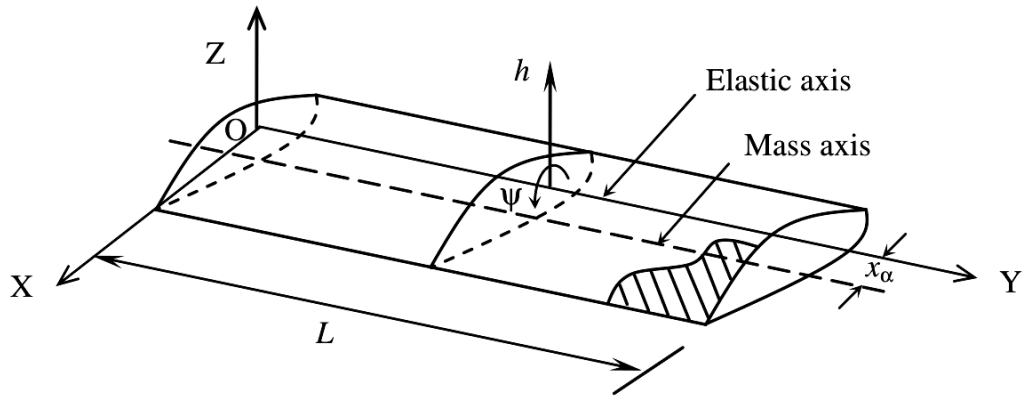

Figure 3.2: The coordinate system and notation for a bending–torsion coupled beam [81]

The wing is idealised as an assembly of bending-torsion coupled beam elements which are governed by the following differential equations in free vibration, see Banerjee [2, 73, 74, 81]

$$EIh'''' + m\ddot{h} - mx_\alpha\ddot{\Psi} + K\Psi''' = 0 \tag{3.14}$$

$$GJ\Psi'' + mx_\alpha\ddot{h} - I_\alpha\ddot{\Psi} + Kh''' = 0 \tag{3.15}$$

where h and Ψ are the transverse displacement (heave) and torsional rotation (pitch) respectively, as shown in Figure 3.2; EI, GJ and K are the bending, torsional and bending-torsion coupling rigidities respectively. m is mass per unit length; I_α represents the mass moment of inertia per unit length and x_α denotes the distance between the mass and elastic axes of the elements.

Note that when a non-uniform aircraft wing is idealised as a collection of bending-torsion coupled beam elements, every element will have different mass (m), inertia (I_α), and stiffness properties (EI, GJ, K). The distance between

mass axis and elastic axis (x_α) can also vary from element to element. In equations (3.14) and (3.15), x_α essentially represents the geometrical coupling arising from the geometry of the cross-section. On the other hand, K represents the material coupling which occurs due to the ply orientation of the composite laminate. For isotropic material, clearly K is zero which reduces the governing differential equation to

$$EIh'''' + m\ddot{h} - mx_\alpha\ddot{\Psi} = 0 \tag{3.16}$$

$$GJ\Psi'' + mx_\alpha\ddot{h} - I_\alpha\ddot{\Psi} = 0 \tag{3.17}$$

3.3 Modal Analysis

The main concept of the modal analysis is to represent the system displacements as a linear combination of the free vibration mode shapes, particularly using the first few modes which are the most important through the use of generalized coordinates. It is instructive to look at the general form of the equations of motion which could be written in the matrix form as follows

$$[M]\{\ddot{q}\} + [K]\{q\} = \{F\} \tag{3.18}$$

In equation (3.18), $[M]$ and $[K]$ are the mass and stiffness matrices, and $\{F\}$ and $\{q\}$ are the force and displacement vectors. The main objective now is to solve equation (3.18) which represents the wing motion in two degrees of freedom namely the heave and pitch. In order to solve the equations, the

normal mode method is used.

In general, if a combination of the first few number of modes in free vibration say N is used, then according to modal approach , i.e. the normal mode method, the displacement vector can be represented by

$$\{q\} = [\phi]\{\eta\} \tag{3.19}$$

where $[\phi]$ is the modal matrix in which each column is an eigenvector of the free vibration analysis resulting from eigen-problem and $\{\eta\}$ is the generalized coordinates. Premultiplying equation (3.18) by $[\phi]^T$ and equation using (3.19) and applying the eigenvectors orthogonality conditions lead to a set of second order ordinary differential equations in terms of generalized coordinates. Each equation is represented by its mode, say the i^{th} mode [95–97] to give

$$\ddot{\eta}_i + \omega_i^2 \eta_i = Q_i; \quad i = 1, 2, \ldots, N \tag{3.20}$$

where

$$Q_i = \{\phi\}_i^T \{F\}$$

$$\omega_i^2 = \{\phi\}_i^T [K] \{\phi\}_i$$

$$1 = \{\phi\}_i^T [M] \{\phi\}_i$$

The modes are normalized in a way such that the generalized mass matrix became an identity or unit matrix. In this work, the structural system is considered as an undamped system.

It is clear from the above equations that to calculate the system displacement vector from equation (3.19), modal matrix $[\phi]$ and the generalized coordinates vector $\{\eta\}$ should be obtained first. Determining the first N modes to formulate the modal matrix $[\phi]$ can be accomplished by the dynamic stiffness method as described in next Section 3.4 for beams or directly by solving the eigen-value problem for the aerofoil case. Then to obtain the generalized displacement vector $\{\eta\}$, equation (3.20) should be solved. It is a second order ordinary differential equation (ODE) in time. Here, it can be solved for example by using numerical integration in the time domain by Runge-Kutta scheme. When seeking solution, equation (3.20) should be reduced to two first order ordinary differential equations (ODE) say, in y_{1i} and y_{2i} by using the transformation $y_{1i} = \eta_i$ and $y_{2i} = \dot{\eta}_i$ give

$$\dot{y}_{1i} = y_{2i} \tag{3.21}$$

$$\dot{y}_{2i} = Q_i - \omega_i^2 y_{1i} \tag{3.22}$$

The system of equations (3.21) and (3.22) can now be solved for each mode i. It is an initial value problem and therefore, the initial conditions for y_{1i}, y_{2i}, $\dot{y}_{1i}$ and $\dot{y}_{2i}$ needs to be specified from the initial values of the generalized coordinates. The general initial conditions are:

$$h(0) = h_0; \qquad \alpha(0) = \alpha_0 \tag{3.23}$$

$$\dot{h}(0) = \dot{h}_0; \qquad \dot{\alpha}(0) = \dot{\alpha}_0 \tag{3.24}$$

In this way,

$$\{\eta_0\} = [\phi]^{-1}\{q_0\} \tag{3.25}$$

$$\{\dot{\eta}_0\} = [\phi]^{-1}\{\dot{q}_0\} \tag{3.26}$$

3.4 DSM of Modal Analysis

The dynamic stiffness method, as mentioned before, is an analytical method to solve the governing equations of a structural system in an exact sense. In this section, a general approach to drive the dynamic stiffness matrix is outlined following the work of Banerjee [98].

Rewriting equation (3.18) in symbolic form for free undamped vibration of a structural system, one cam write

$$L(q) = 0 \tag{3.27}$$

where L and q are the differential operator and the corresponding displacement vector respectively. Equation (3.27) can be solved analytically by assuming that the displacement is harmonically varying according to the expression

$$\{q\} = \{q_a\}e^{i\omega t} \tag{3.28}$$

where q_a is the displacement amplitude, ω is circular or angular frequency and t is time. Substituting of equation (3.28) into (3.27) will eliminate the time

dependent term to give

$$L_1(q_a, \omega) = 0 \tag{3.29}$$

where L_1 is a differential operator. The general solution for equation (3.29) can be sought in the form

$$\{q_a\} = [A]\{C\} \tag{3.30}$$

where $\{C\}$ is a constant vector and $[A]$ is a frequency dependent square matrix. In order to get a relationship between the force and displacement, the boundary conditions should be applied for both forces and displacements resulting from equation (3.30). First the displacement boundary condition is applied to give

$$\{\delta\} = [B]\{C\} \tag{3.31}$$

In equation (3.31), $\{\delta\}$ represents the nodal displacements and $[B]$ is a square matrix obtained by substituting the displacement boundary conditions in $[A]$ of equation(3.30). Then applying the boundary conditions for forces lead to

$$\{F\} = [D]\{C\} \tag{3.32}$$

where $\{F\}$ is the force vector and $[D]$ is a square matrix obtained from $[A]$ of equation(3.30). Then with the help of equations (3.31) and (3.32), the constant vector $\{C\}$ can be eliminated to give

$$\{F\} = [D][B]^{-1}\{\delta\} = [DS]\{\delta\} \tag{3.33}$$

where $[DS]$ is the frequency dependent dynamic stiffness matrix. It is a symmetric square matrix which is a functions of frequency and other structural parameters. After formulating $[DS]$ matrix, the problem leads to a non-linear eigen-value problem to compute the natural frequencies and modes of the system. The most accurate and efficient way to solve this problem is to use the Wittrick-Williams algorithm [62], which is capable of converging upon the natural frequencies of the system with certainty.

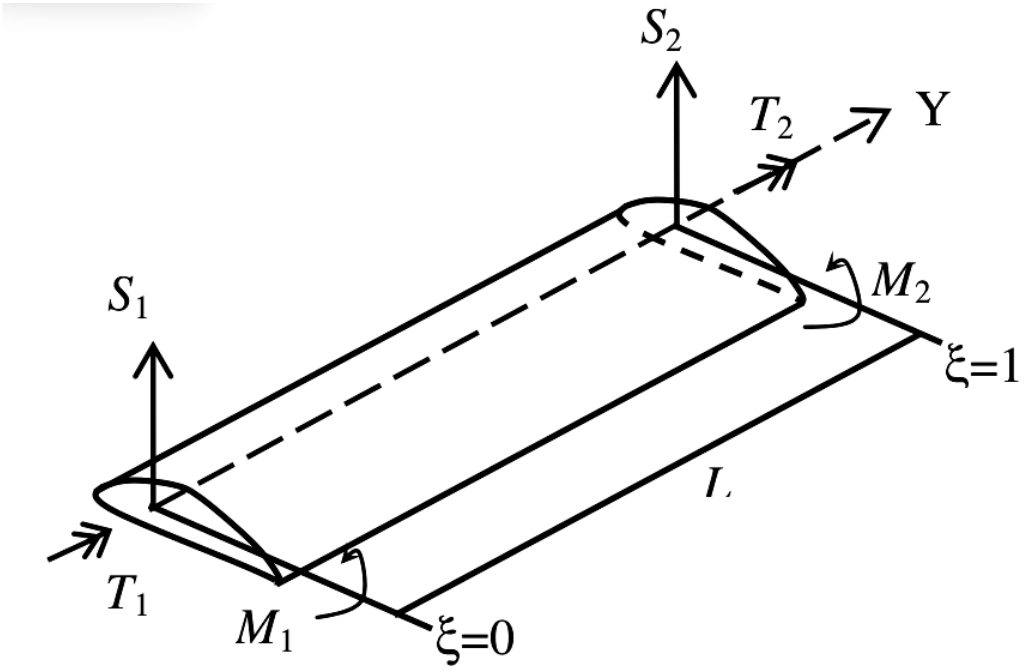

Figure 3.3: Nodal forces for a bending–torsion coupled beam [81]

For composite beams with the inclusion of both material and geometrical coupling, the complete derivation and formulation of the dynamic stiffness matrix can be found in [81] which is used in this work. Referring to Equation (3.33) and Figure 3.3, the force vector $\{F\}$ is formulated as,

$$\{F\} = [S_1 \;\; M_1 \;\; T1 \;\; S_2 \;\; M_2 \;\; T_2]^T \tag{3.34}$$

where S, M and T are the shear, bending moment and torsion respectively at node 1 and 2. $[D]$ is 6×6 matrix defined as,

$$[D] = \begin{bmatrix} [D_{11}] & [D_{12}] \\ [D_{21}] & [D_{22}] \end{bmatrix} \tag{3.35}$$

with

$$[D_{11}] = \begin{bmatrix} -\alpha^2 e_\alpha g_\alpha k_b W_3 & \alpha p_\alpha W_3 & -\beta^2 e_\beta g_\beta k_b W_3 \\ -p_\alpha W_2 & \alpha e_\alpha g_\alpha k_b W_2 & p_\beta W_2 \\ -q_\alpha W_1/L & \alpha e_\alpha g_\alpha W_1/L & q_\beta W_1/L \end{bmatrix}$$

$$[D_{12}] = \begin{bmatrix} -\beta p_\beta W_3 & -\gamma^2 e_\gamma g_\gamma k_b W_3 & -\gamma^2 p_\gamma W_3 \\ -\beta e_\beta g_\beta k_b W_2 & p_\gamma W_2 & -\gamma e_\gamma g_\gamma k_b W_2 \\ \beta e_\beta g_\beta W_1/L & q_\gamma W_1/L & \gamma e_\gamma g_\gamma W_1/L \end{bmatrix}$$

$$[D_{21}] = \begin{bmatrix} \alpha(\alpha e_\alpha g_\alpha k_b C_{h\alpha} - p_\alpha S_{h\alpha})W_3 & \alpha(\alpha e_\alpha g_\alpha k_b S_{h\alpha} - p_\alpha C_{h\alpha})W_3 & \beta(\beta e_\beta g_\beta k_b C_\beta - p_\beta S_\beta)W_3 \\ (p_\alpha C_{h\alpha} - \alpha e_\alpha g_\alpha k_b S_{h\alpha})W_2 & (p_\alpha S_{h\alpha} - \alpha e_\alpha g_\alpha k_b C_{h\alpha})W_2 & -(\beta e_\beta g_\beta k_b S_\beta + p_\beta C_\beta)W_2 \\ (q_\alpha C_{h\alpha} - \alpha e_\alpha g_\alpha S_{h\alpha})\frac{W_1}{L} & (q_\alpha S_{h\alpha} - \alpha e_\alpha g_\alpha C_{h\alpha})\frac{W_1}{L} & -(q_\beta C_\beta + \beta e_\beta g_\beta S_\beta)\frac{W_1}{L} \end{bmatrix}$$

$$[D_{22}] = \begin{bmatrix} \beta(p_\beta C_\beta + \beta e_\beta g_\beta k_b S_\beta)W_3 & \gamma(\gamma e_\gamma g_\gamma k_b C_\gamma - p_\gamma S_\gamma)W_3 & \gamma(p_\gamma C_\gamma + \gamma e_\gamma g_\gamma k_b S_\gamma)W_3 \\ (\beta e_\beta g_\beta k_b C_\beta - p_\beta S_\beta -)W_2 & -(\gamma e_\gamma g_\gamma k_b S_\gamma + p_\gamma C_\gamma)W_2 & -(p_\gamma S_\gamma - \gamma e_\gamma g_\gamma k_b C_\gamma)W_2 \\ (\beta e_\beta g_\beta C_\beta - q_\beta S_\beta)\frac{W_1}{L} & -(q_\gamma C_\gamma + \gamma e_\gamma g_\gamma S_\gamma)\frac{W_1}{L} & -(q_\gamma S_\gamma - \gamma e_\gamma g_\gamma C_\gamma)\frac{W_1}{L} \end{bmatrix}$$

and

$$[B] = \begin{bmatrix} 1 & 0 & 1 & 0 & 1 & 0 \\ 0 & \alpha/L & 0 & \beta/L & 0 & \gamma/L \\ -e_\alpha g_\alpha/L & e_\alpha/L & e_\beta g_\beta/L & e_\beta/L & e_\gamma g_\gamma/L & e_\gamma/L \\ C_{h\alpha} & S_{h\alpha} & C_\beta & S_\beta & C_\gamma & S_\gamma \\ S_{h\alpha}\alpha/L & C_{h\alpha}\alpha/L & -S_\beta\beta/L & C_\beta\beta/L & -S_\gamma\gamma/L & C_\gamma\gamma/L \\ u^*_\alpha/L & v^*_\alpha/L & u^*_\beta/L & v^*_\beta/L & u^*_\gamma/L & v^*_\gamma/L \end{bmatrix} \tag{3.36}$$

Apart from inverting $[B]$, calculating all the above matrices is computationally very efficient. There are many common terms between these matrices which are functions of the material properties and geometric parameters of the beam [81].

3.4.1 Mode Shapes

Solving the non-linear eigen-value problem in the frequency domain by using the Wittrick-Williams algorithm to obtain the natural frequencies is essential to compute the mode shapes of the system. These mode shapes are usually obtained by assuming one of the degrees of freedom to be fixed and possibly equal to unity, and then estimating the remaining degrees of freedom in terms of the chosen one. However, this procedure sometimes imposes a great challenge because the choice of arbitrary chosen displacement at a node is not unique.

The modal matrix $[\phi]$ in section 3.3 has to be mass normalized to reduce the system to the form given in equation (3.20). Otherwise, a constant coeffi-

cient will appear in each term of equation (3.20). Therefore, the mass matrix $[M]$ is required in order to obtain the normalized mode shapes $[\phi]$ from the unnormalized mode shape $[\psi]$. However, the DSM reduces the system to one frequency dependent matrix $[DS]$ instead of two matrices; namely mass matrix $[M]$ and stiffness matrix $[K]$ as in FEM. Thus, $[M]$ is not calculated by default.

The solution for this problem is now to compute the mass matrix $[M]$ numerically from the dynamic stiffness matrix $[DS]$. The dynamic stiffness matrix is sought to be composed of both $[K]$ and $[M]$ as proposed by Leung [99],

$$[DS(\omega)] = [K] - \omega^2[M] \tag{3.37}$$

Equation (3.37) is essentially the relation between the dynamic stiffness matrix and the mass and stiffness matrices. By computing $[DS(\omega)]$ in equation (3.37) for any two frequencies; ω_i and ω_j

$$[DS(\omega_i)] = [K] - {\omega_i}^2[M] \tag{3.38}$$

$$[DS(\omega_j)] = [K] - {\omega_j}^2[M] \tag{3.39}$$

Then the mass matrix could be obtained by subtracting equations (3.38) and (3.38) as

$$[M] = \frac{1}{{\omega_j}^2 - {\omega_i}^2}[DS(\omega_i) - DS(\omega_j)] \tag{3.40}$$

For better accuracy ω_i and ω_j must be small numbers. Finally, the mass

normalize modes are calculated as follows,

$$\{\psi_i\}^T[M]\{\psi_i\} = m_i \tag{3.41}$$

$$\{\phi_i\} = \{\psi_i\}/\sqrt{m_i} \tag{3.42}$$

Another critical point worth mentioning here, is the coupling between modes. In general, the sign of the mode shape has no significance, however in the case of bending-torsion beam, it is important. The essential point here is to keep the relative relation between the bending and torsion mode shapes for each natural frequency. Furthermore, special care should be taken with the sign convention of the system and to make sure that it matches the aerodynamic model. A new code (using Python programming language) has been developed to compute these modes and it has been extensively validated. This code has been implemented using Object-Oriented Programming paradigm based on DSM, Appendix B.

3.5 Fluid Structure Coupling

As mentioned before, strongly coupled interaction is considered in this study. Two levels of coupling are evident for which the first one is essentially time coupling carried out by integrating the aerodynamic forces over the wing at every time step to calculate the force vector $\{F\}$. The second level of interaction is coupling between the structural displacements and the fluid solver. For the case in hand where the wing cross section is considered to be rigid (non-deformable), the wing surface displacement will be updated at every time step

according to the calculated values of the lift force and the pitching moment about the elastic axis. By knowing h and α from equation (3.19) the new location P_1 for point P_0 on the wing is obtained from

$$\{P_1\} = [R]\{P_0\} + \{h\} \tag{3.43}$$

where $\{h\}$ is the displacement vector in the plunging direction and $[R]$ is the rotation matrix involving an angle α around the elastic axis. For a wing section normal to the xy-plane, the rotation matrix by an angle α in radian around a unit vector in the z direction through the elastic axis is

$$[R] = \begin{bmatrix} cos\alpha & -sin\alpha & 0 \\ sin\alpha & cos\alpha & 0 \\ 0 & 0 & 1 \end{bmatrix} \tag{3.44}$$

There is still an essential point worth mentioning here which is the coupling between the three dimension CFD mesh and the one dimension beam model. This has been achieved by creating an intermediate coarse mesh. This coarse mesh is created by dividing the wing into number of element as shown in Figure 3.4. The CFD mesh cells lay in an element of the intermediate mesh, their pressure values are integrated over this element area [100]. Then, the essentially resultant force and moment about the beam node can be calculated which are the aerodynamic forces [97]. These forces are represented by the right-hand side $\{F\}$ in equation (3.18).

Once the displacement of each beam node is calculated, the CFD mesh of

the wing surface is updated according to equation (3.43) at each time step. This approach allows the CFD mesh and structure mesh to be independent. Also, this is computationally efficient because the displacement is calculated only at the beam nodes and extrapolated for the rest of the CFD mesh cell centres as required leading to much finer than the intermediate mesh.

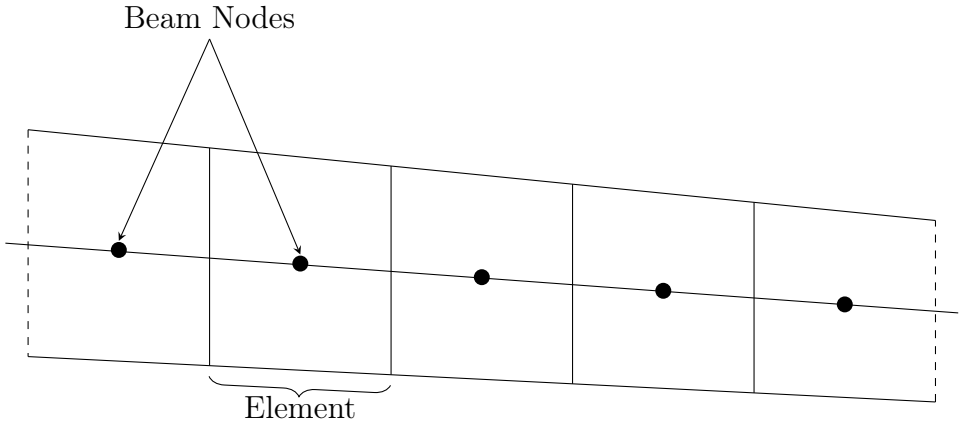

Figure 3.4: Intermediate mesh for coupling

Chapter 4

Free Vibration and Flutter Characteristics of High Aspect-ratio Aircraft Wings

The free vibration characteristics of two types of high aspect ratio aircraft wings of metallic construction are presented in this chapter, namely, that of sailplane type and that of transport airliner type. In each case, the wing is idealised as an assembly of bending-torsion coupled beams using the dynamic stiffness method of modelling leading to a nonlinear eigenvalue problem as described in Chapter 3. The problem is solved by applying the Wittrick-Williams algorithm yielding natural frequencies and mode shapes. The computed natural frequencies and mode shapes are compared and contrasted for the two type of aircraft wings. The objective of this study is to demonstrate the variation in natural frequencies and mode shapes of different aircraft wings. Additionally, a flutter analysis based on classical flutter theory is presented and the effect of

modes truncation is highlighted. The results presented in this chapter follow the earlier work of Banerjee et al. [1, 2].

4.1 Free Vibration Analysis

In an aircraft, the wings are the principal load-carrying structures which provide the necessary lift for the air vehicle [13, 15]. For sailplanes and transport airliners, the wings are designed to have high aspect ratios to generate sufficient lift. When compared with the fuselage, the bending and torsional stiffnesses of the wing are much lower. Understandably, for this reason the wings are considered to be the most vital and sensitive parts of an aircraft. In many applications, the wings are treated as cantilevered on the side wall of the fuselage. It is worth mentioning that for an aircraft wing the bending and torsional deformations are generally coupled due to non-coincident mass and shear centres as well as due to material coupling in case of composite wings.

Additionally, the engine mass and inertia mounted on a transport aircraft wing can have significant effects on the model behaviour and hence must be taken into account in the analysis. Thus the presence of the engine on the wing can influence the flutter behaviour significantly. Generally, the engine is idealised as concentrated lumped mass and inertia located at some distance from a particular node on the wing. The off-set connection of the mass and inertia of the engine away from the node on the wing flexural axis can also be significant.

4.2 Geometrical and Material Properties

As mentioned earlier, two highly contrasting categories of aircraft, namely, sailplanes and transport airliners are analysed for their free vibration characteristic. For each category, designated letters **S** for sailplane and **T** for transport airliner are used. Two aircraft models **S1** and **S2** for sailplanes, while **T1** and **T2** for transport airliners, whose main geometrical configurations and particulars are given in Table 4.1 are modelled using the dynamic stiffness method. It is clear that the two aircraft in the same category share quite similar, but not identical properties. However, the properties of one category are very different from the other. So it is expected that the free vibration and flutter behaviour of the same category of aircraft may have similar features, whereas that of different categories will be dissimilar.

It is to be noted that there is one engine on each wing for the transport aircraft **T1** whereas there are two engines on each wing for the transport aircraft **T2**. By contrast, the sailplanes **S1** and **S2** have no engines (see Table 4.1).

Geometrical parameters	Sailplane		Transport airliner	
	S1	**S2**	**T1**	**T2**
Span(m)	15	22	29.24	40.4
Wing area(m^2)	10.05	15.44	90.00	162.1
Aspect ratio	22.39	31.35	9.5	10.08
Wing root chord (m)	0.85	0.90	5.35	4.88
Wing tip chord (m)	0.35	0.36	1.42	2.54
Sweep angle ($^\circ$)	0	0	27.6	0
No. of engines	0	0	1	2

Table 4.1: Geometrical properties of two types of aircraft wings.

4.3 Natural frequencies and mode shapes

The first six natural frequencies for the two categories of the aircraft were computed using CALFUN-B [74]. These are shown in Table 4.2 for all the four aircraft. The natural frequency values are labelled with B, T or C indicating bending dominated (B), torsional dominated (T), and bending/torsional coupled (C) modes, respectively. The mode shapes corresponding to the natural frequencies of the two types of aircraft are illustrated in Figs. 4.1 and 4.2 respectively. Note that the bending displacements are shown by blue solid lines, whereas the torsional rotations are shown by red dashed lines.

Frequencies (rad/s)	Sailplane		Transport airliner	
	S1	**S2**	**T1**	**T2**
ω_1	13.512(B)	10.657(B)	19.710(B)	11.524(B)
ω_2	42.686(B)	42.594(B)	55.288(B)	33.085(B)
ω_3	95.025(B)	109.837(B)	100.248(B)	45.420(C)
ω_4	165.137(T)	111.651(T)	120.907(C)	87.857(B)
ω_5	171.375(C)	201.303(B)	197.742(C)	97.761(T)
ω_6	281.683(B)	261.204(T)	248.250(T)	121.521(T)

(B)– Bending dominated; (T)–Torsional dominated; (C)– Bending/torsional coupled

Table 4.2: Natural frequencies of two types of aircraft wings.

4.3.1 Sailplanes S1 and S2

It can be seen from Table 4.2 that natural frequencies for the two sailplanes are different, but quite similar. An inspection of the two sets of mode shapes in Figure 4.1 suggests that the first three modes of the two sailplanes are bending dominated whereas the fourth one for each of the two sailplanes is a pure torsional mode. It should be noted that the sailplane wings are made up

of two parts, the inner wing and the outer wing, and they are connected by a solid metallic rod. As a consequence, the mass and inertia distributions near the junction between the inner and the outer wings will be discontinuous and nonuniform. This is reflected in some of the mode shapes shown in Figure 4.1.

4.3.2 Transport Airliners T1 and T2

The results in Table 4.2 show that the natural frequencies of transport airliner **T1** are higher than those of **T2**. One of the reasons for this difference can be attributed to the fact that the transport airliner **T2** has a much higher aspect ratio than **T1**. It is worth-noting that there are more coupled modes in this category of aircraft than the previous one. This is mainly due to the significant separation between the mass and elastic axes, and also due to the presence of the engine(s) on the wing. For sailplanes S1 and S2, this separation was small because of the short chord and long wing. The mode shapes for **T1** and **T2** shown in Figure 4.2 reveal some interesting features. The first three modes of **T1** are primarily bending modes, whereas the fourth, fifth and sixth modes are coupled in bending and torsion. The coupling between the bending and torsional motions in these three latter modes is mainly due to the outboard engine and the elastic axis locations.

As for the transport airliner **T2**, the first, second and fourth modes are bending dominated, whilst the other three are coupled modes exhibiting relatively more torsional deformation than bending.

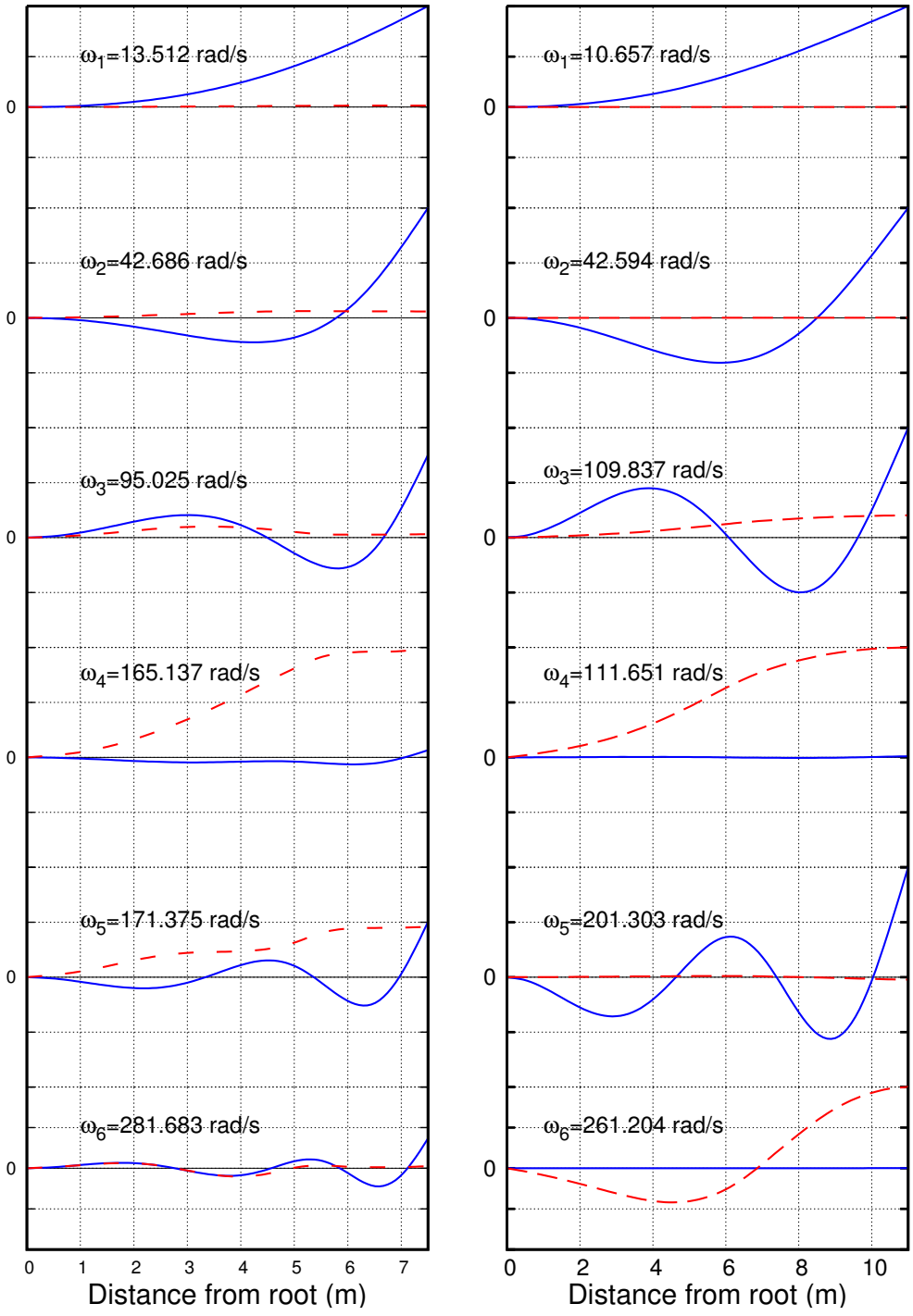

(a) Sailplane-**S1** **(b)** Sailplane-**S2**

Figure 4.1: Natural frequencies and mode shapes of sailplane wings. —— bending displacement; – – – torsional displacement.

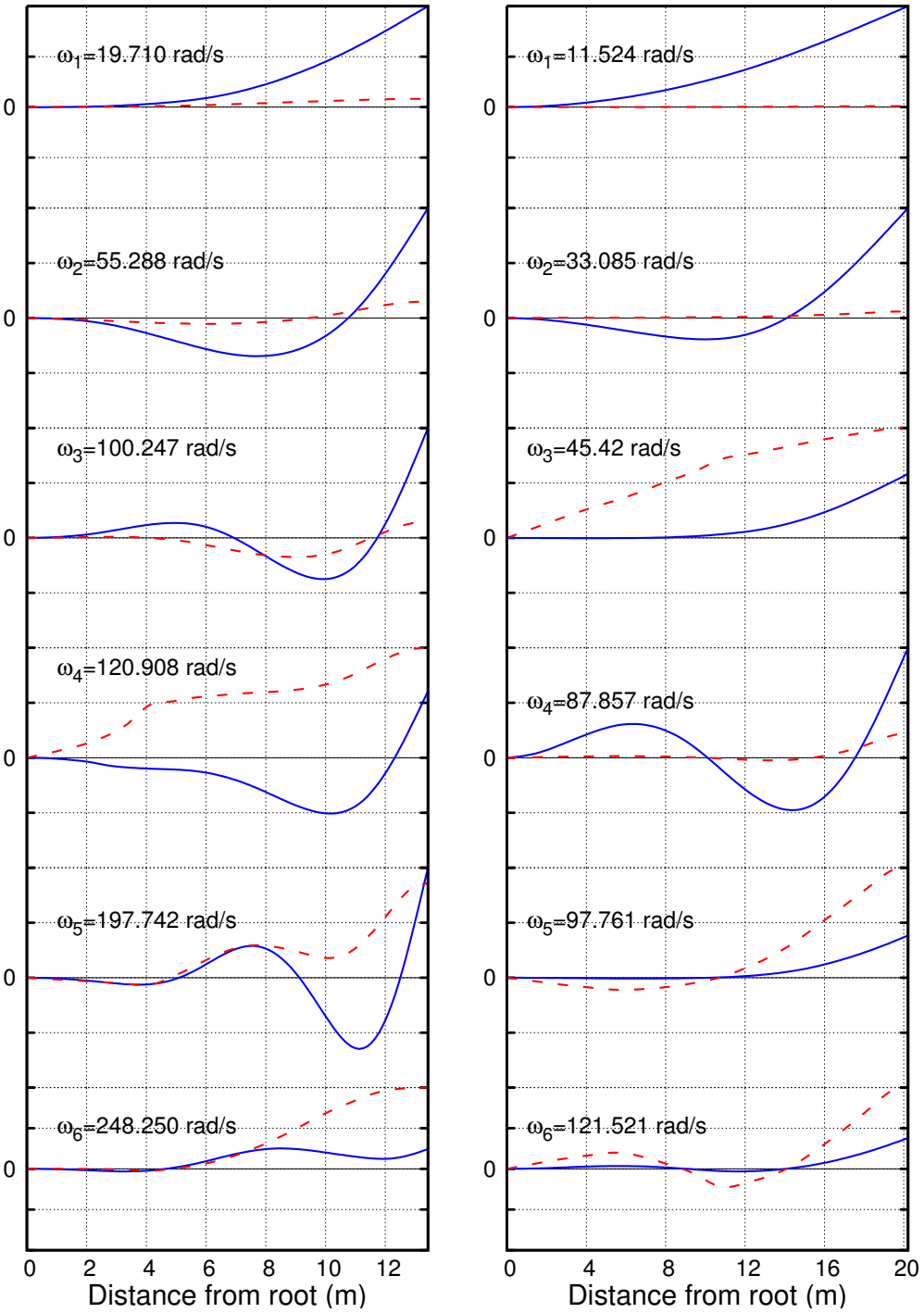

(a) Transport airliner-**T1** **(b)** Transport airliner-**T2**

Figure 4.2: Natural frequencies and mode shapes of transport airliner wings. —— bending displacement; – – – torsional displacement.

4.4 Flutter Analysis

After carrying out the modal analysis to establish the first six natural frequencies and mode shapes of the two types of the aircraft wings in the previous section, the next step is to use the results to predict the flutter point. In order to achieve this, the software CALFUN-B [74] is used.

Since the flutter determinant is a highly complex function involving the air speed V and frequency ω, it was necessary to search for the zero of the flutter determinant both in terms of its real and imaginary parts. The search is carried out in a two dimensional plane using air speed V and frequency ω as variables to ensure that the real and imaginary parts of the flutter determinant and hence the whole flutter determinant are zeros. From a computational point of view, a range of airspeeds and frequencies are chosen. Then for a fixed airspeed (V), the real and imaginary parts of the flutter determinant are computed for a range of frequencies, and next, the process is repeated for a range of airspeeds until the whole flutter determinant is zero.

Using the above classical procedure, the flutter speed and the flutter frequencies of all the four aircraft are computed and shown in Table 4.3. As can be seen from the results in Table 4.3, the flutter speeds of **S1** and **S2** are quite similar (77.02 m/s for **S1** and 71.02 m/s for **S2**) although the flutter frequencies are somehow different (76.51 rad/s for **S1** and 53.67 rad/s for **S2**).

With regard to the results of the two transport airliners, **T1** has a flutter speed of 406.25 m/s whereas that of **T2** is 251.10 m/s. The corresponding flutter frequencies are 78.39 rad/s and 28.70 rad/s respectively. Further, checks

to confirm the flutter point which are beyond the scope of this work have been reported in [1, 2].

Critical values for flutter	Sailplane		Transport airliner	
	S1	**S2**	**T1**	**T2**
Flutter speed $V_f(m/s)$	77.02	71.02	406.25	251.10
Flutter frequencies $\omega_f(rad/s)$	76.51	53.67	78.39	28.70

Table 4.3: The flutter speeds and frequencies of the two types of aircraft wings by using CALFUN-B

4.4.1 The Effect of Mode Number Truncation

The above flutter analysis for the four different aeroplanes are based on the first six natural modes. These first six modes are a combination of bending dominated, torsional dominated and coupled modes. They have been used in the previous analysis to ensure accurate predication of the flutter speed and frequency. Hence, the classical flutter analysis is computationally less expensive compared to using CFD, using six or even modes for flutter analysis is computationally affordable. In this section, a flutter analysis of **T1** based on the first three and four modes is presented. The results will be compared and contrasted against the previous study which carried out using the first six modes.

The transport airliner **T1** was chosen for this study because it has a distinctive mode shape characteristics. As show in Figure 4.2a, the first three modes are pure bending and the torsional effect appears starting from the forth mode. Table 4.4 lists the flutter speed and frequency based on the first three, four and six natural modes. The results show that, using only the first

three modes is not enough to predicted the flutter point at all. This can be attributed to the fact that the first three modes are bending dominated modes. In order to pinpoint the flutter point, the first torsional dominated mode must be included in the analysis. Also, the results based on four modes are quite different compared to using the first six modes. This could be due to coupled nature of the fifth modes.

Critical values for flutter	Number of Modes		
	3	4	6
Flutter speed $V_f(m/s)$	—	595.63	406.25
Flutter frequencies $\omega_f(rad/s)$	—	88.04	78.39

Table 4.4: The flutter speeds and frequencies of the transport airliner **T1** using CALFUN-B

4.5 Summary

The fundamental characteristics of free vibration natural modes of two types of aircraft have been investigated, namely sailplanes and transport airliner. Two different models of each type have been studied and contrasted. This study reveals the significance of the natural modes of aircraft wings and how these modes inherently capture the essential characteristics of the system. Moreover, a classical flutter analysis has been carried out for the four aircraft with a deep focus on the transport airliner **T1** which showed a sensitivity to the selected mode shapes. This confirms that the importance of including at least one torsional mode in order to predict the flutter boundary.

Chapter 5

Typical Two-dimensional Aerofoil-section Model

In this chapter a number of different cases for two-dimensional aerofoil-section models will be investigated to test the source code developed using OpenFOAM [101]. A wide range of operating conditions is considered to ascertain the potential of the method presented in this study. Some results from this chapter have been published by Kassem et al. [3, 5].

5.1 Case A: Pitching NACA 0012 Aerofoil

The subsonic flow over pitching NACA 0012 airfoil was first examined. The aerofoil was forced to oscillate about its quarter chord when the angle of attack oscillates with time according to equation (5.1) below. In this equation, α and α_m are the instantaneous angle of attack (as a function in time t) and the mean angle of attack, respectively. This pitching oscillation has amplitude α_A

and frequency ω. The fluid flow is considered to be inviscid and therefore, the governing equations of flow are reduced to Euler equations, see chapter 3. The flow conditions are selected in conformity with the research carried out by Yang [102]. Important parameters are summarized in Table 5.1. Although the free stream Mach number is chosen to be 0.301, the flow is considered to be compressible. It is reported [102, 103] that the flow will accelerate near the transonic speed region due to the aerofoil shape and movement. In the present case, the flow was first modelled at fixed angle of attack equal to α_m (static mesh). Then these static flow field results were used as initial conditions for the forced pitching oscillation case (dynamic mesh). The `snappyHexMesh` utility of OpenFOAM was used to generate the mesh. A very large domain was created for this case to test the `snappyHexMesh` $30c \times 10c$ with $118,379$ grid cell where c is the chord of the aerofoil. Figure 5.1 shows part of the mesh around the aerofoil showing different levels of grid refinement around it. Furthermore, Figure 5.2 shows the mesh cells around the aerofoil trailing edge which has a small finite thickness. The instantaneous angle of attack $\alpha(t)$ can be written as

$$\alpha(t) = \alpha_m + \alpha_A sin(\omega t) \tag{5.1}$$

where α_m, α_A and ω have been defined before.

Figure 5.3 shows the coefficient of lift versus the angle of attack. The predicted results by OpenFOAM are in good agreement with the experimental measurements [103] as well as with the Euler code used by Yang et al. [102].

Description	Variable	Value
Aerofoil		NACA 0012
Mean angle of attack	α_m	4.93°
Angle of attack amplitude	α_A	±4.99°
Free stream Mach number	M_∞	0.301
Reynolds number	Re	3.91×10^6
Reduced frequency	k	0.198
Pitch axis from leading edge	x_p	25% of chord

Table 5.1: Characteristics of test case A.

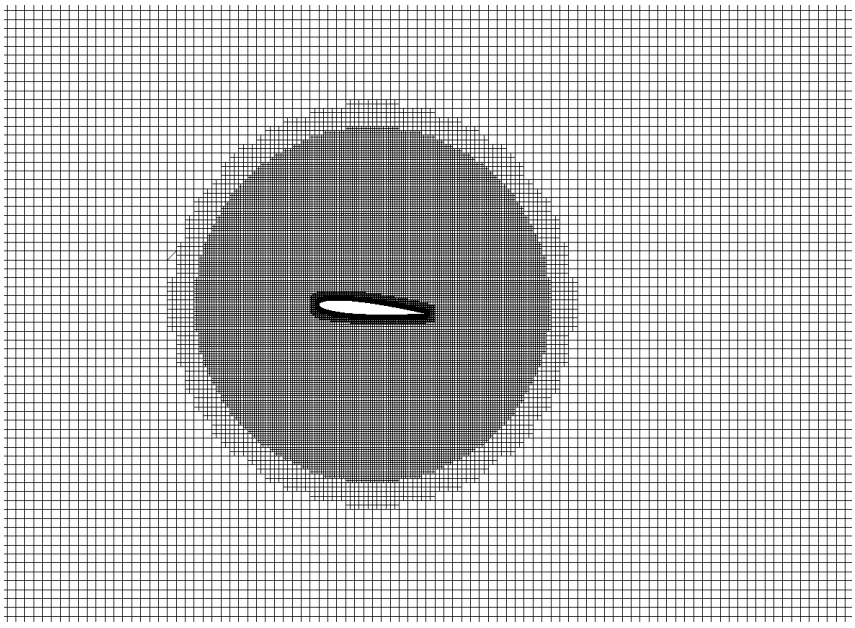

Figure 5.1: Part of the mesh around NACA 0012.

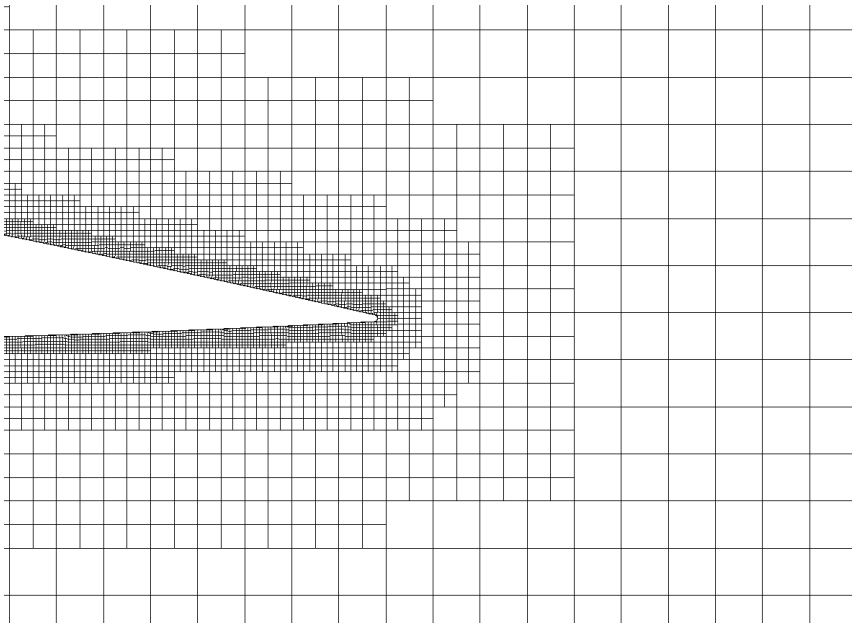

Figure 5.2: Mesh around NACA 0012 tail.

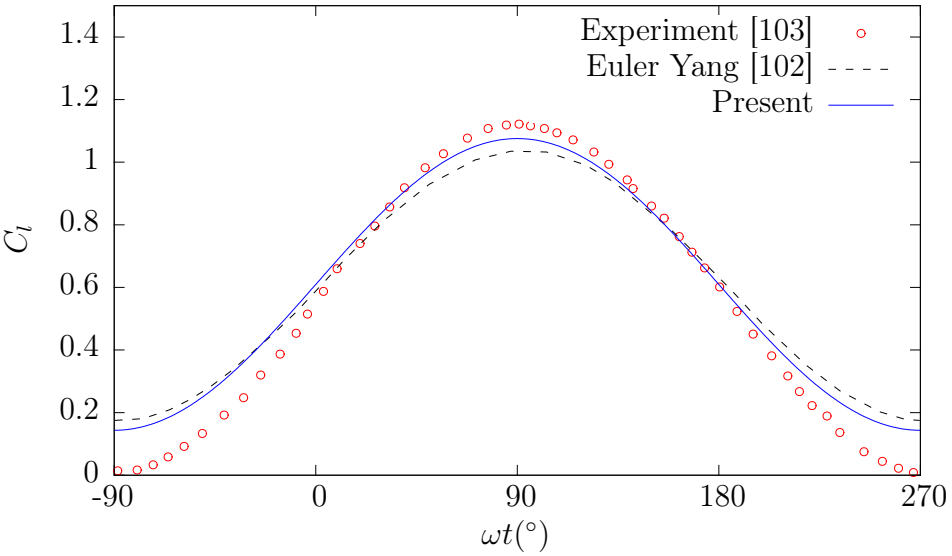

Figure 5.3: Instantaneous lift Coefficient

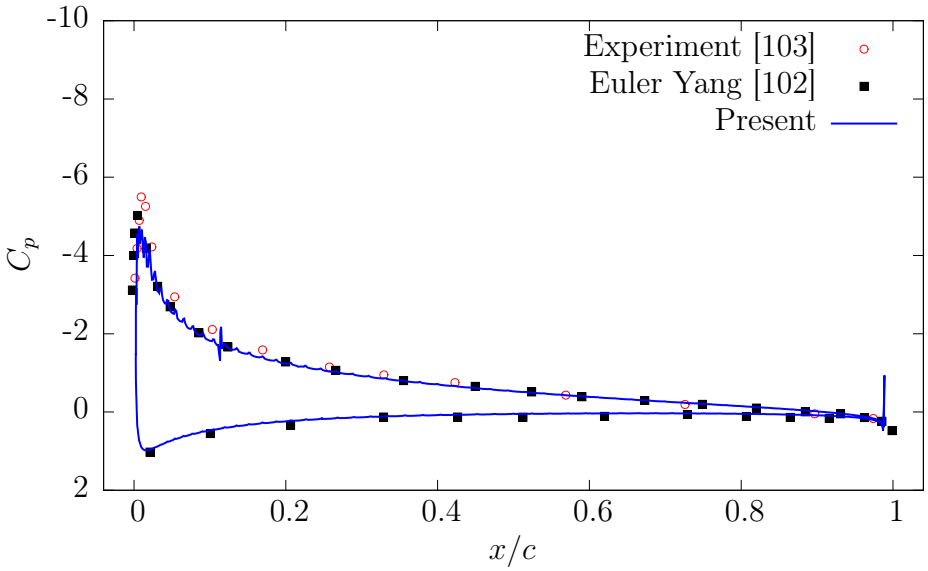

Figure 5.4: Pressure distribution at instance of $(c_p)_{min}$

Furthermore, the pressure coefficient is also compared in Figure 5.4 against the same references. Although Figure 5.4 shows good agreement along the aerofoil, the pressure distribution at the leading edge shows some differences. This was also observed and reported by McCroskey et al. [103]. The boundary layer is generally fully attached under this conditions. However, a separation bubble appears near the leading edge which leads to flow transition. This could be the possible reason for the disagreement in results with experiment around the leading edge.

5.2 Case B: Pitching NACA 64A010 Aerofoil

The second test case (case B) is a pitching aerofoil about the quarter chord in transonic flow free stream. The aerofoil section is NACA 64A010. This particular case is one of the widely used cases in the literature to validate transonic CFD codes. The experimental work was carried out by Davis [104],

Alonso et al. [95] as well as by Chen et al. [105] in order to validate their CFD codes. Table 5.2 gives the operating conditions for this case. Such parameters lead to free stream velocity $270m/s$ at standard sea level conditions ($\rho = 1.225kg/m^3$).

Description	Variable	Value
Aerofoil		NACA 64A010
Mean angle of attack	α_m	0°
Angle of attack amplitude	α_A	$\pm 1.01^\circ$
Free stream Mach number	M_∞	0.8
Reynolds number	Re	1.256×10^7
Reduced frequency	k	0.202
Pitch axis from leading edge	x_p	25% of chord

Table 5.2: Characteristics of test case B.

In this case GMSH has been used [106] instead of using one of OpenFOAM meshing utilities. GMSH has a graphical user interface which gives more control, and thus accelerates the mesh generation process. Figures 5.5 and 5.6 show the complete mesh and the mesh around the sharp trailing edge respectively. The computational domain is $15c \times 10c$ with $39,006$ grid cells.

Figure 5.7 shows the lift coefficient versus the angle of attack. The results from this work are in good agreement with the experimental results [104]. Although this figure shows an excellent agreement along the pitching cycle, it also shows that the model did not predict very well the peak points. In general, these results are comparable with the results reported in literature [95, 105]. McMullen et al. [107] modelled this case with a grid independent study and also reported under and over predictions for the lift coefficients. Obviously, increasing the grid quality will increase the accuracy, but it is not the main

reason for these differences. The differences are probably due to ignoring the viscous effect for a streamed-line objects like aerofoils. In such cases the forces arising from shear stress may have a noticeable contribution. More investigations using different grids and turbulence models might be needed to clarify and pin-point the exact reason. Figure 5.8 shows the Mach contours at the maximum angle of attack.

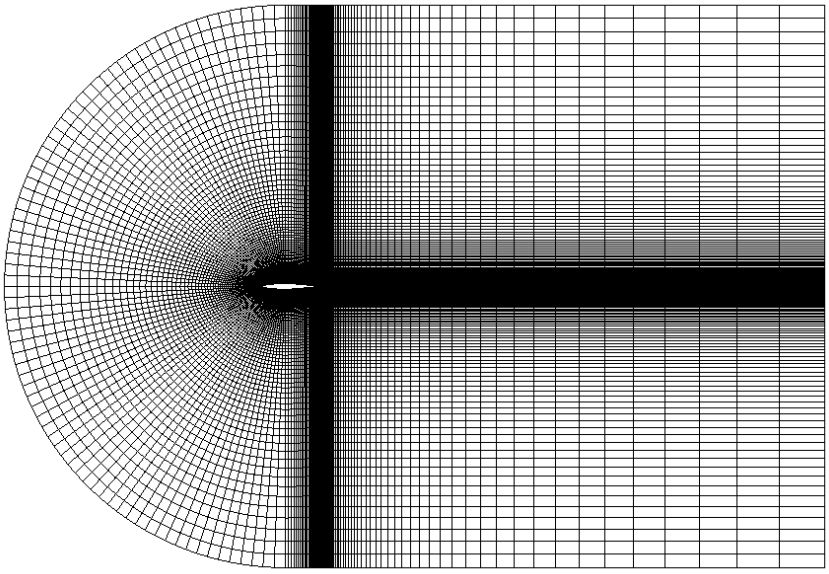

Figure 5.5: C-mesh type around NACA 64A010

5.3 Case C: Self-Sustained NACA 64A010 Aerofoil

In this case, the modal analysis was used to calculate the aerofoil displacement. Again the NACA 64A010 was used as in case B. However, three different operating conditions are modelled for this case [95]. The newly developed `elasticDisplacement` library in OpenFOAM was used, see Appendix A. Table 5.3 shows the selected operating conditions. The structural model follows the one which was introduced by Isogai [17, 18]. The modelling for each con-

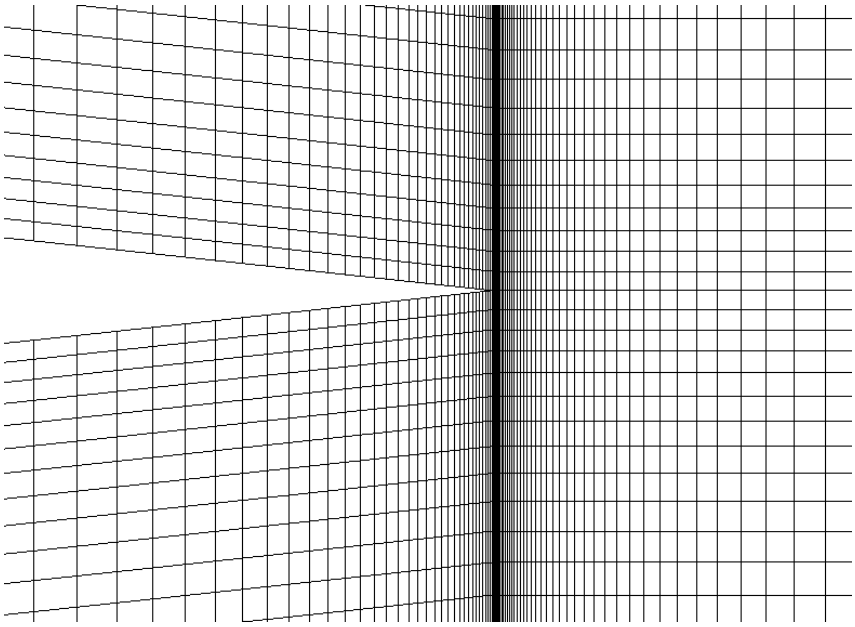

Figure 5.6: Mesh around NACA 64A010 tail

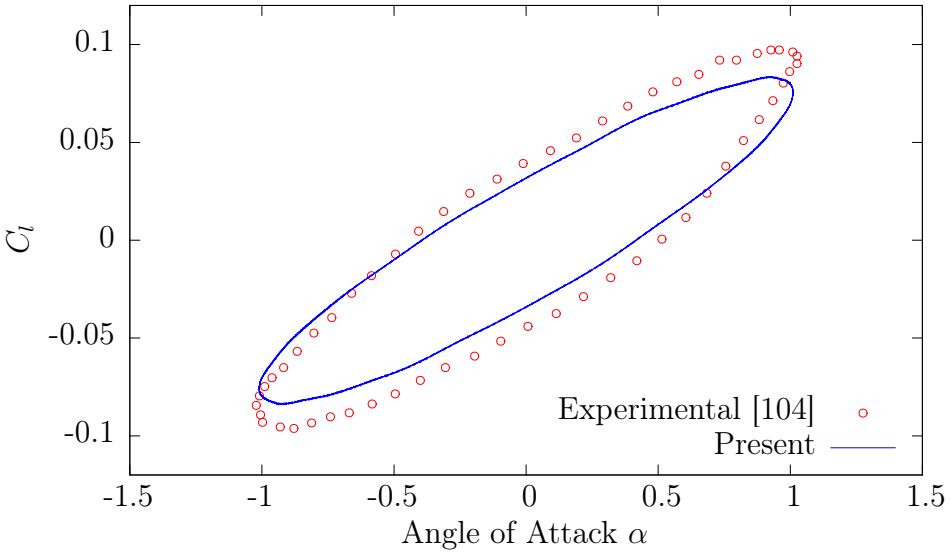

Figure 5.7: Instantaneous lift Coefficient

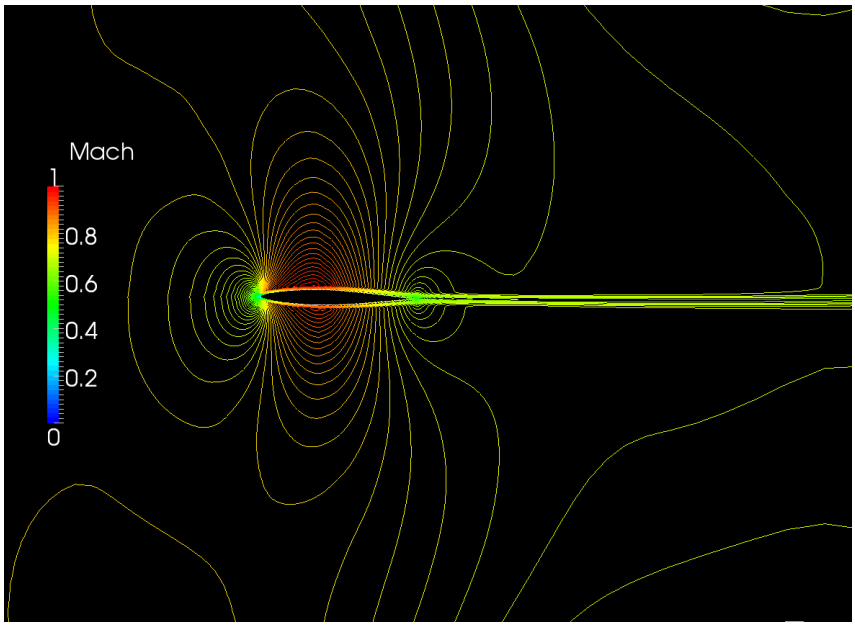

Figure 5.8: Mach Contours at $\alpha = 1.01°$

dition was done using three stages, namely, fixed aerofoil, pitching aerofoil around the elastic axis and finally self-sustained aerofoil. The same mesh from case B was used to save computational time. A fifth-order Runge-Kutta with adaptive time step developed by Cash and Karp [108] was selected. It is basically one of the OpenFOAM ODE solvers for non-stiff systems.

Description	Variable	Value
Aerofoil		NACA 64A010
Mean angle of attack	α_m	$0°$
Angle of attack amplitude	α_A	$\pm 1.01°$
Free stream Mach number	M_∞	$0.85, 0.825, 0.875$
Speed Index	$V^* = \frac{U_\infty}{\omega_\alpha b \sqrt{\mu}}$	0.439, 0.612, 1.420
Free stream velocity	U_∞	170, 237, 545 m/s
Aerofoil mass ratio	μ	60
Reynolds number	Re	1.256×10^7
Static unbalance	x_α	1.8
Squared radius of gyration	r_α^2	3.48
uncoupled natural freq. in plunge	ω_h	100 rad/s
uncoupled natural freq. in pitch	ω_α	100 rad/s
Pitch axis from leading edge	x_p	-50% of chord

Table 5.3: Characteristics of test case C.

Figures 5.9, 5.10 and 5.11 show the responses and the forces for the three operating conditions. It is clear that Figure 5.9 represents a damped response, whereas Figure 5.11 shows a divergent response. Both are in very good agreement with [95, 105]. It was expected that Figure 5.10 would predict the flutter point as reported by Alonso et al. [95], but as it turned out, the flutter point was missed only by a small margin. Nevertheless, the trend to predict the flutter speed is sufficiently clear.

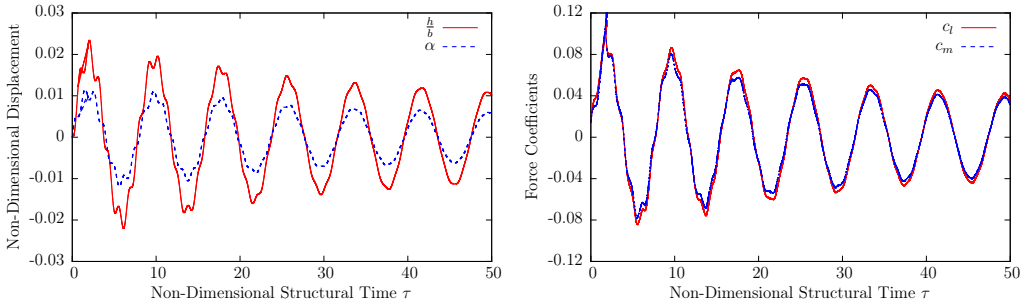

(a) Displacements. **(b)** Force Coefficients.

Figure 5.9: Damped Response. $M_\infty = 0.85$, $V^* = 0.439$

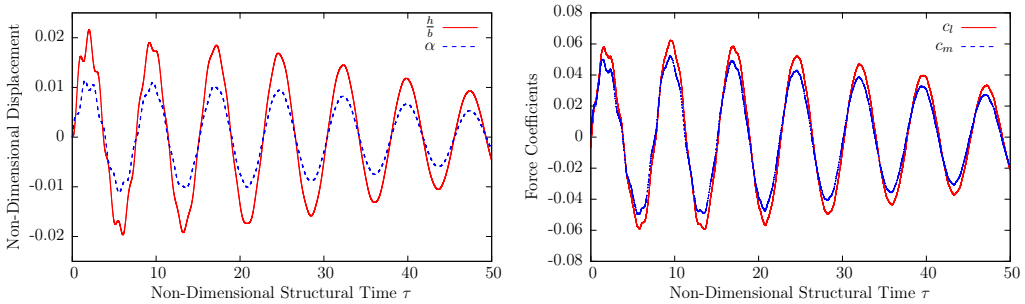

(a) Displacements. **(b)** Force Coefficients.

Figure 5.10: Damped Response. $M_\infty = 0.825$, $V^* = 0.612$

5.4 Summary

In this chapter three case studies for two different aerofoils have been carried out in order to validate the core functionality of OpenFOAM and its suitability

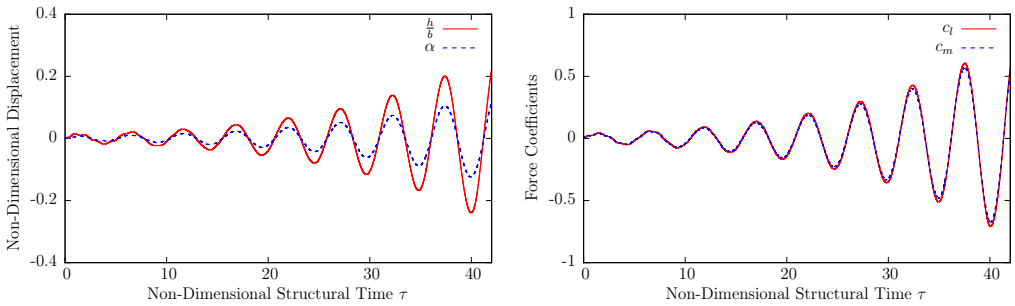

(a) Displacements. **(b)** Force Coefficients.

Figure 5.11: Divergent Response. $M_\infty = 0.875$, $V^* = 1.420$

for aeroelastic analysis. The first case study is for subsonic flow over pitching NACA0012. The meshing capabilities, fluid solver and more importantly the dynamic mesh solver were tested thoroughly which proved to be fit for this study. The second case is for transonic flow over oscillating NACA64A010 which showed good agreement with experimental data. The final case is for self-sustained NACA64A010 in different flow conditions. The aerofoil elastic model was used in this case and the CFD results were contrasted against other numerical results from the literature. All the case studies showed good agreement, which paved the way for further investigation by implementing the complete wing model.

Chapter 6

Aircraft Wing Model

The main case study in this chapter is the analysis of the well-known Goland wing (without store), incorporating its "Heavy" version which has been featured in the literature several times [109–113]. It is a rectangular wing, but has a parabolic aerofoil cross-section as assumed by earlier investigators. In this thesis, this wing is considered to be made of both metallic and composite materials independently. For the composite wing different values for the material coupling coefficient K are considered in the analysis. Some of the results presented in this chapter have been published earlier by Kassem et al. [4].

6.1 Metallic Goland Plus Wing

In this section two cases will be investigated to confirm the correctness of the newly developed source code. Both cases are for metallic Goland wing. The first case is focussed on forced pitching oscillation and the second case is about the elastic response to predict the transonic flutter. A wide range of operating

conditions is modelled to demonstrate the potential of the method. It is worth noting that the Goland wing considered here is a much heavier version of the original Goland wing [114]. This version of Goland wing was introduced by Eastep and Olsen [109] as a suitable model for transonic flutter case study. The properties of this wing are given in Table 6.1.

Property	Value
Chord, c	$1.829\ m$
Semispan, s	$6.096\ m$
Thickness to chord ratio,	0.04
Mass, M	$534.7\ kg/m$
Bending stiffness, EI	$9.789 \times 10^6\ Nm^2$
Torsional stiffness, GJ	$0.989 \times 10^6\ Nm^2$
Mass moment of inertia, I_α	$129.5\ kgm$

Table 6.1: Goland Wing Properties

6.1.1 Case A: Goland Wing in Pitching Motion

The first test case (case A) is a pitching rigid Goland wing in transonic flow with free stream Mach no 0.92, amplitude 0.5° and frequency 3.0 Hz. These values were selected based on the operating conditions reported in Refs. [110–112] which are subsequently used to compare results of the current investigation.

The mesh was generated using GMSH software [106] instead of using one of the OpenFOAM meshing utilities. Figures 6.1 shows the mesh around the wing cross-section and Figure 6.2 shows the rectangular wing surface mesh with dimensions. The computational domain is taken as $30c \times 10c \times 10c$ with $169,380$ grid cells (c being the chord of the wing). Despite the fact that the

mesh used here is coarse compared to previous studies for this case [110–112], the predicted results are found to be in excellent agreement with published results in the literature as illustrated in Figure 6.3, which shows results for the moment coefficient (C_m) versus the lift coefficient (C_l). In order to obtain mesh independent solution and more stable simulations, a finer mesh $(242,400)$ cells has later been used to carry out the flutter analysis. Moreover, a number of cases have been compared with the results from a much finer grid $(454,800$ cells) to make sure that the results are mesh independent which means that the results are reliable and sufficiently accurate. In this comparison, it should be noted that CAPTSD is a three-dimensional, transonic, small-disturbance solver based on potential-flow equations and ENS3DAE gives an inviscid Euler solution [111]. OpenFOAM results in Figure 6.3 represent the present study and those coming from the Fluent commercial software. Fluent results are for inviscid Euler solution using unstructured mesh which was reported in [110]. Figure 6.4 shows the Mach number field around the wing which is a good indication of the presence of the shock waves. The wide range of Mach numbers chosen from subsonic to supersonic is one of the main features of transonic flow which is captured by the model.

6.1.2 Case B: Flutter Analysis

In this case, the modal analysis was used to calculate the wing displacement as described in section 3.3. In order to apply the modal analysis and run the developed code, the free vibration modes were computed using the wing mass and stiffness properties. CALFUN-B code [74] was used to obtain the natural

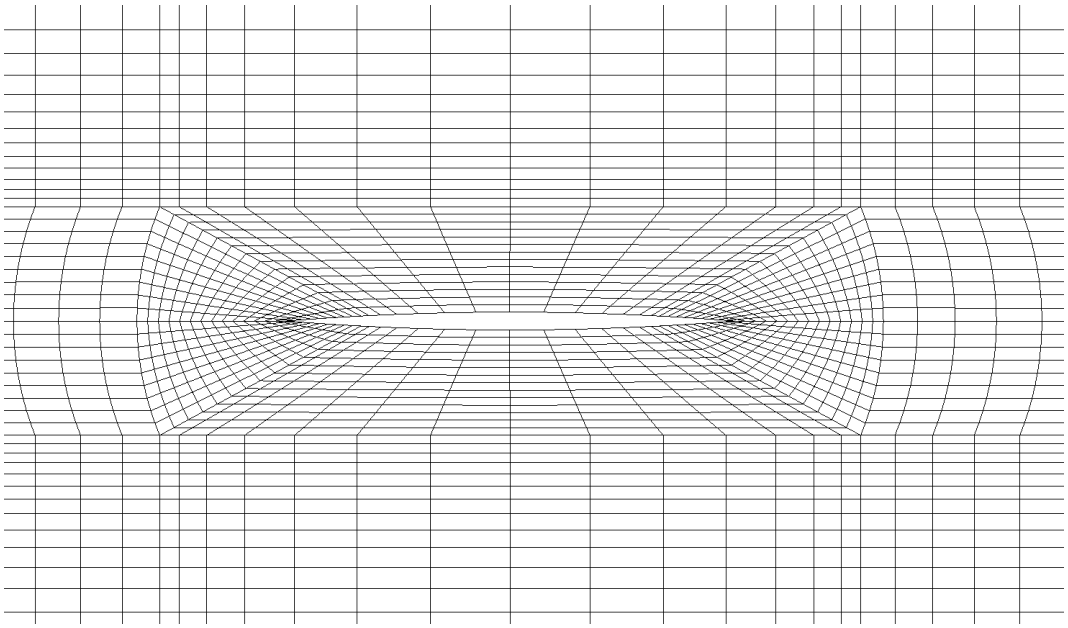

Figure 6.1: Mesh around Goland wing cross-section

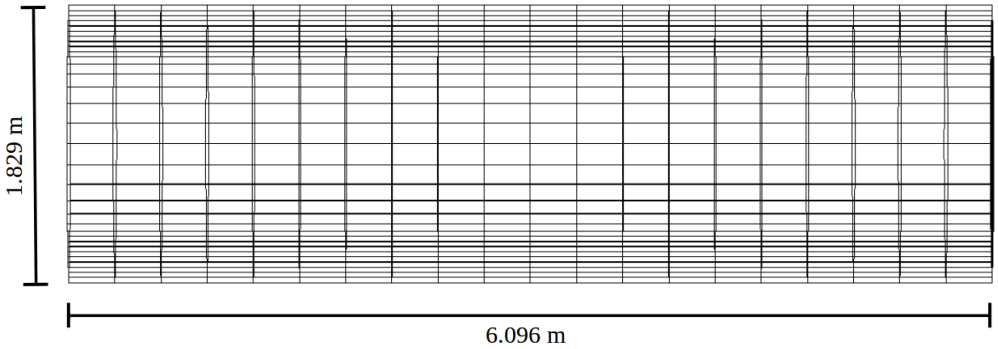

Figure 6.2: Goland Wing Surface Mesh

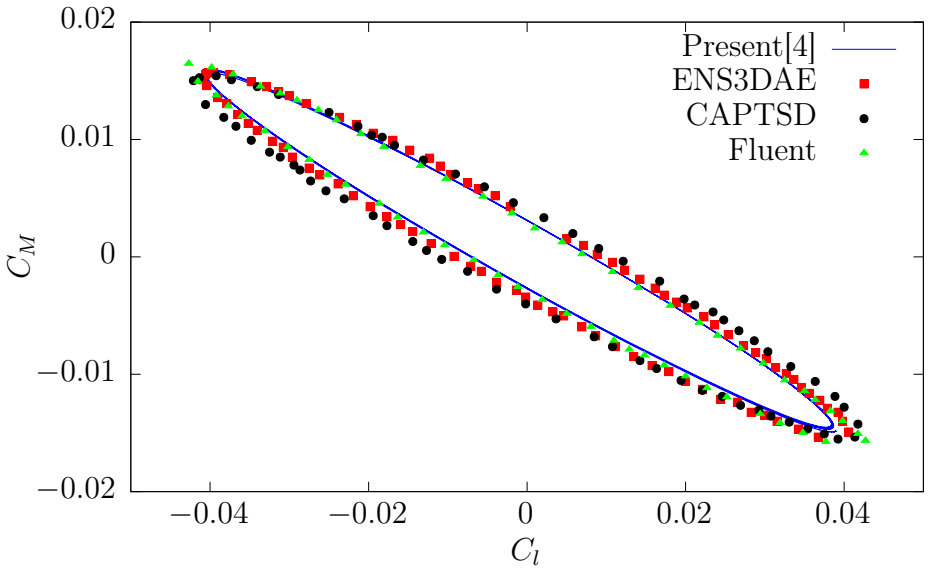

Figure 6.3: Moment Coefficient verses Lift Coefficient

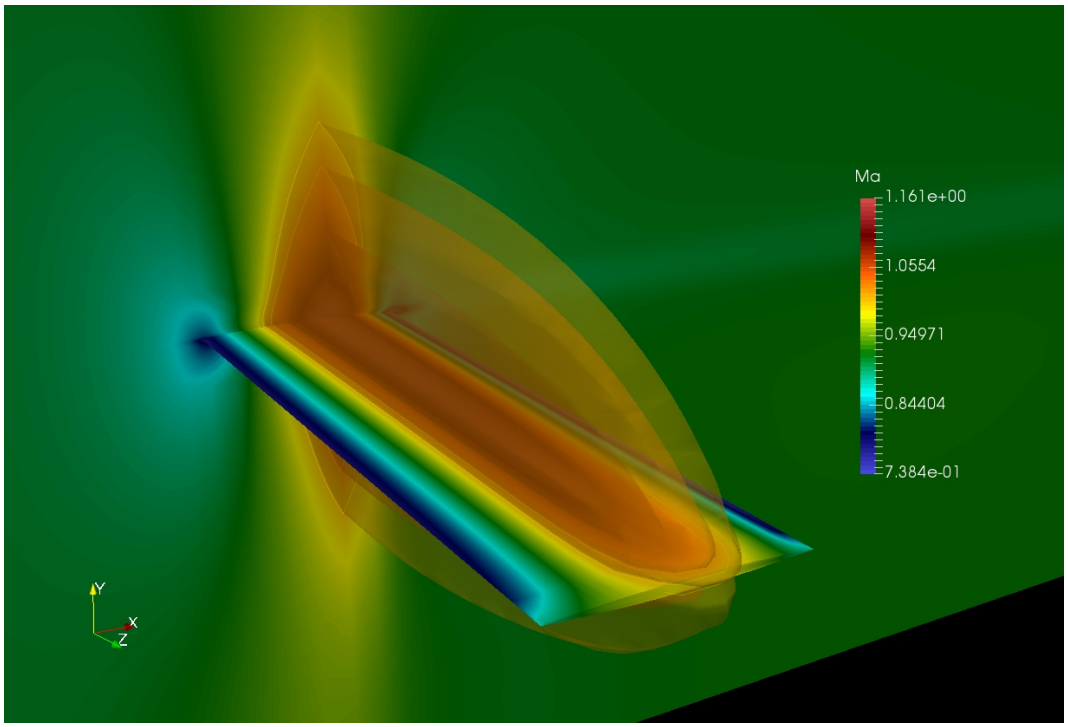

Figure 6.4: Mach Number Contours.

modes which are based on the dynamic stiffness method descried in section 3.2. Figure 6.5 shows the normalized natural modes of the Goland wing (metallic) idealised as a cantilever beam. It is clear that the first mode is predominantly bending and the second mode is predominantly torsional mode, whereas the third and forth modes are heavily coupled in bending and torsion. This is consistent with results from Chapter 4. The computed natural frequencies are compared with those from previous studies as shown in Table 6.2.

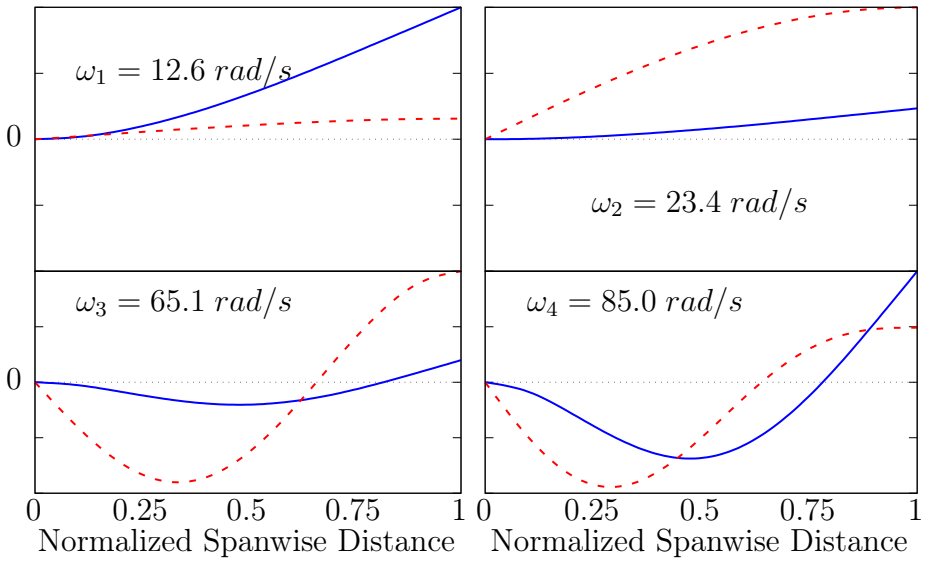

Figure 6.5: Free Vibration Modes for Metallic Goland Wing.—— bending displacement; – – – torsional displacement.

Mode	Natural Frequencies (Hz)			
	CALFUN-B	Beran [111]	NASTRAN (1D Beam)[115]	Chung [115]
1st Mode	2.01	1.97	1.95	1.93
2nd Mode	3.73	4.05	4.08	3.92
3rd Mode	10.36	9.65	-	-
4th Mode	13.53	13.4	-	-

Table 6.2: Natural Frequencies of Metallic Goland Wing (Hz)

The next step is to model the dynamic response based on the computed

modes in order to compute the flutter velocity for a range of Mach numbers. For each test case, non-matched-point flow conditions were used. This means that the Mach number and velocity boundary conditions are selected independently. Then, based on fixed density (1.225 $kg/m3$), temperature (288.15 K) and specific heat ratio (1.4) values at standard-day, sea-level condition, other operating conditions such as the pressure, specific heat capacity and the specific gas constant were calculated [110–112]. In other words, the speed of sound in the model is adjusted for each simulation according to Mach number and the free stream velocity.

Each case was modelled for fixed rigid wing first, until convergence is achieved and then the results were used as initial condition for the flow field. Finally, the structure was perturbed with initial velocity at the wing tip. Figure 6.6 shows the predicted flutter boundary with comparative results from the literature [109, 112, 113]. Therefore, the close proximity of results confirms the predictable accuracy and correctness of the present analyses. The four points in Figure 6.6 predicted by the current OpenFOAM analysis were based on around 15 different simulation at the indicated four Mach numbers and a wide range of free stream velocities. It worth mentioning here that the classical flutter theory using CALFUN-B could not find the flutter point of this case. This could be due to the fact that this case is parametrised for transonic region which beyond the scope of CALFUN-B.

A selective few responses at $M_\infty = 0.8$ are highlighted in Figures 6.7, 6.8 and 6.9. Figure 6.7 shows the generalized displacement of sub-critical response which is dominated by the first mode. After increasing the velocity gradually

and keeping the Mach number fixed, a self-sustained oscillating response was obtained around $V_\infty = 110\ m/s$, see Figure 6.8. It is clear from Figure 6.8 that the first mode is dominating the response. Finally, Figure 6.9 shows the heave response near the wing tip at different free stream velocities which clearly demonstrate the changes in both phase and amplitude of the dynamic response.

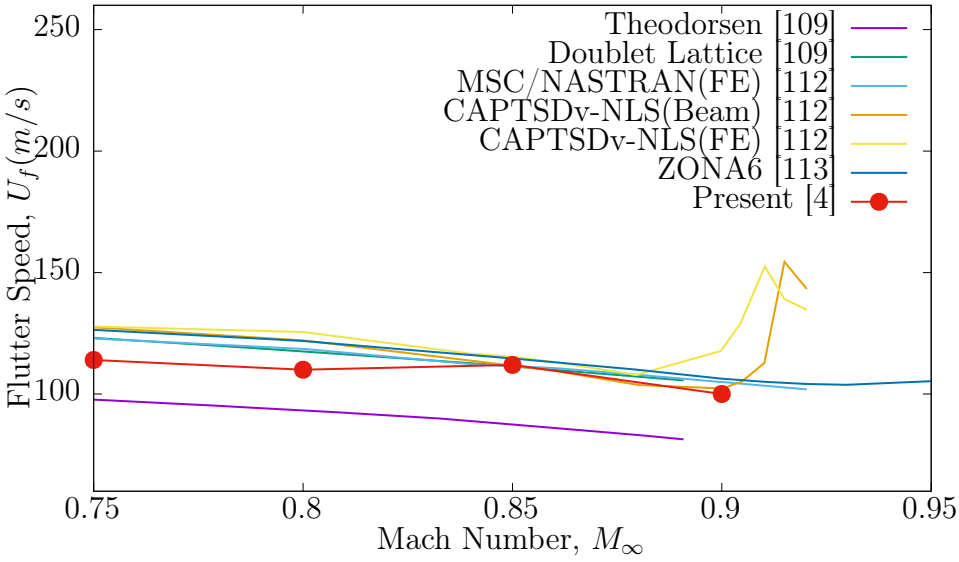

Figure 6.6: Flutter boundary for Goland Wing

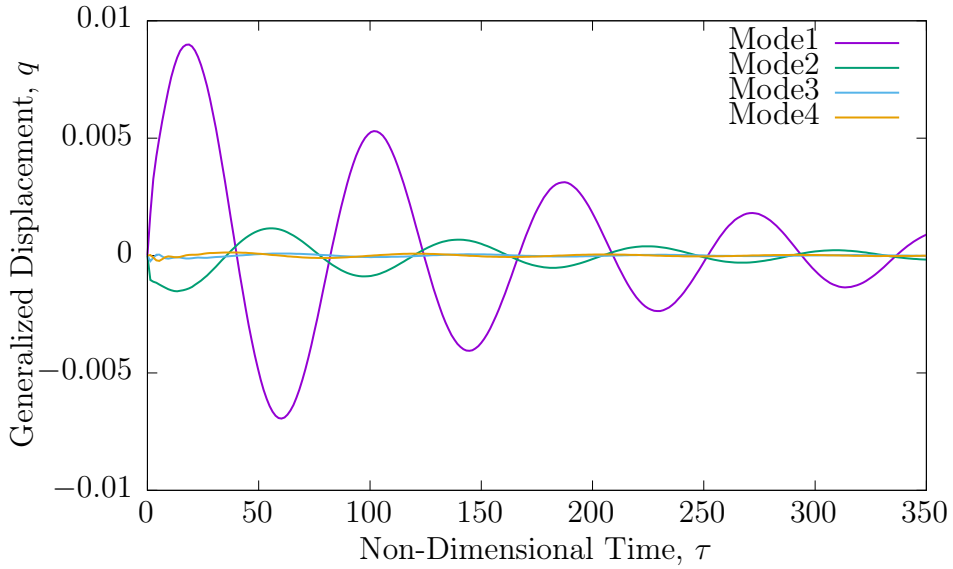

Figure 6.7: Damped Response. $M_\infty = 0.8$, $V_\infty = 80m/s$

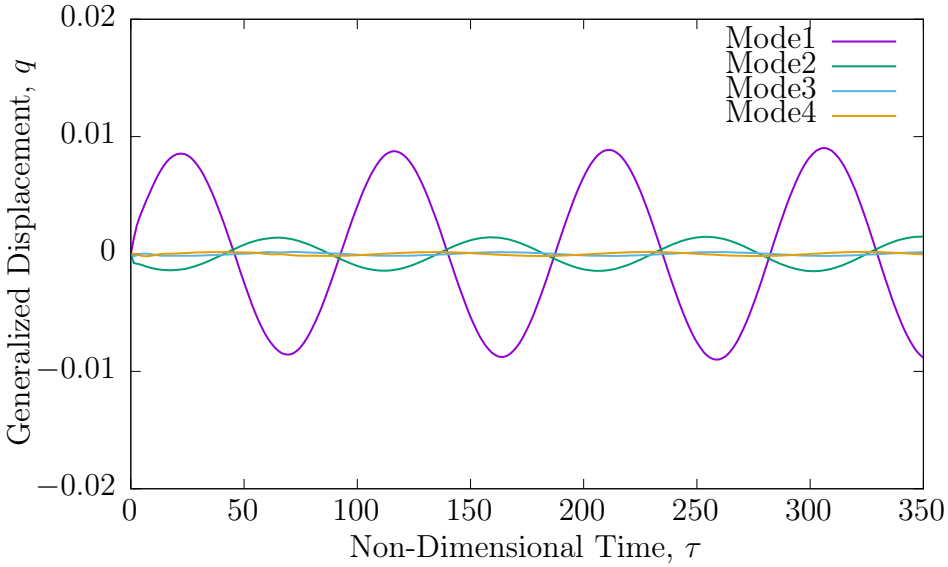

Figure 6.8: Near flutter point Response. $M_\infty = 0.8$, $V_\infty = 110m/s$

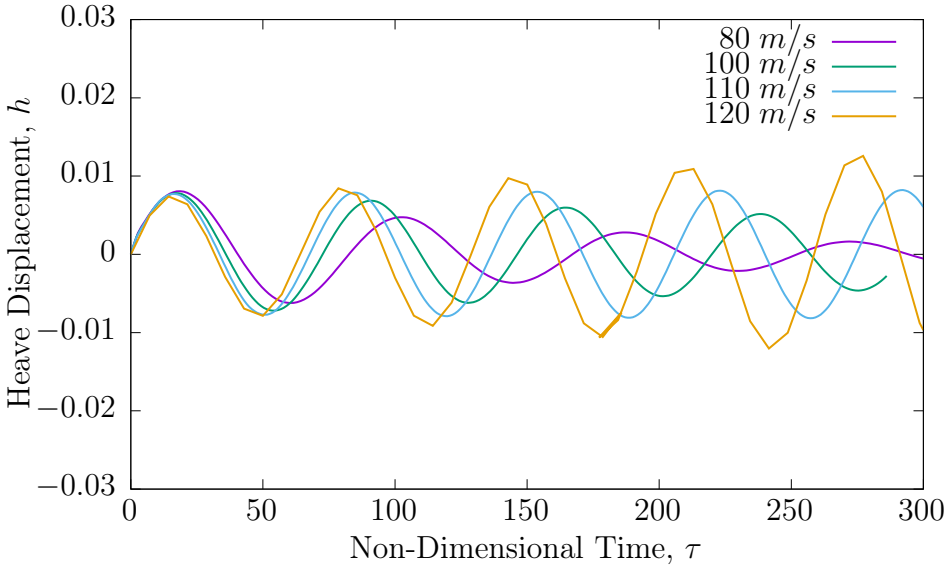

Figure 6.9: Heave Response of the tip, $M_\infty = 0.8$

6.2 Composite Goland Plus Wing

This section investigates the effect of using composites on the dynamic characteristics of the wing. In particular, the effect of material coupling due to the ply orientation of the composite laminate on the flutter speed are given precedence in the investigation.

6.2.1 Natural Frequencies

Using the same geometrical and material properties of Goland wing from Table 6.1, but by considering the material coupling stiffness K within the range of $-2.5\,MN.m^2$ to $2.5\,MN.m^2$. It is the same range reported by Banerjee et al. [81] to study the light version of Goland wing. The material coupling stiffness K is due to the ply orientation of the composite laminates, therefore K value could be adjusted by choosing the ply orientation sequence of the composite.

Figure 6.10 shows the variation of the first four natural frequencies against the material coupling stiffness parameter K. The zero value of K represents the isotropic wing conditions from Section 6.1.2. It is clear from these results that the material coupling has larger effect on the higher modes that the lower ones. These results have been computed using a newly developed code using Python, see Appendix B.

Table 6.3 shows the computed natural frequencies over a wide range of material coupling stiffness parameter K. Also, the geometrical coupling is considered but was kept fixed for all cases. The metallic wing natural frequencies in Table 6.3 are in an excellent agreement with the results of CALFUN-B

in Table 6.2. This comparison validates the accuracy of the newly developed code. Moreover, it demonstrates the consistency of the governing equations and the robustness of the dynamic stiffness method. Once the selected value for K equals to zero, the computed frequencies are equal to those computed by the isotropic version of Goland wing. Essentially the formulation is reduced to metallic material without any extra numerical treatment. This demonstrates the generality of the method and its capability of handling both isotropic and non-isotropic material without implementing two different versions of the code.

Mode	Natural Frequencies (Hz)						
	Material Coupling Coefficient $K[MN.m^2]$						
	-2.5	-2.0	-1.5	0.0	1.5	2.0	2.5
1st Mode	1.21	1.58	1.83	2.01	1.60	1.35	1.01
2nd Mode	3.29	3.48	3.52	3.73	4.08	4.14	3.90
3rd Mode	6.50	8.13	9.46	10.35	7.87	6.72	5.50
4th Mode	9.00	11.14	12.00	13.52	14.36	12.31	9.33

Table 6.3: Natural Frequencies of Heavy Goland Wing for different K values (Hz)

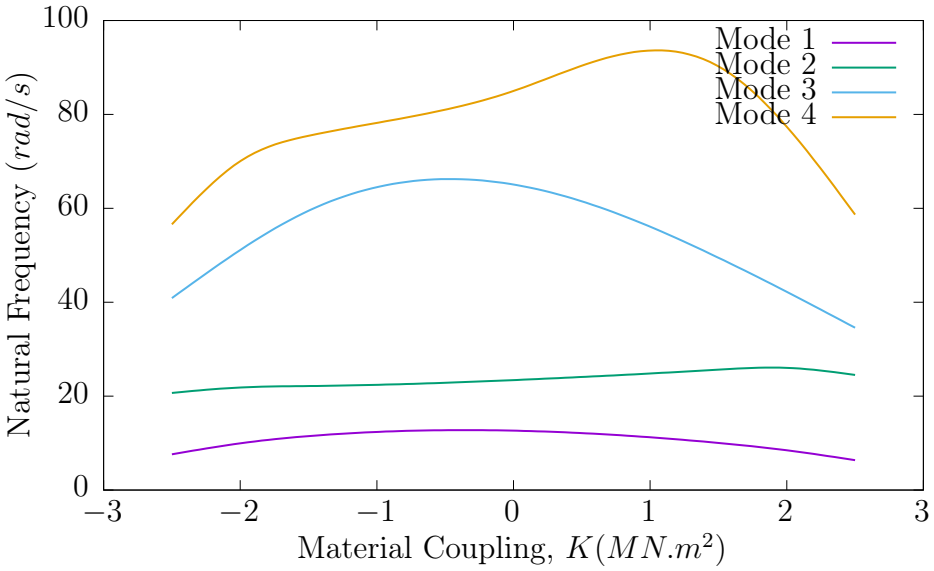

Figure 6.10: Natural frequencies of composite Goland wing.

6.2.2 Mode Shapes

As expected the fundamental difference between the mode shapes for metallic and composite wing is due to the presence of the coupling stiffness parameter K. In particular, the coupling between bending and torsion is prevalent in composite wings arising from the anisotropic nature of fibrous composites in addition to the inertial coupling that exists due to the noncoincident of mass and flexural axes (geometric coupling) . Figure 6.11 shows the effect of both material and geometric coupling on the mode shapes. For metallic Goland wing the first mode was a pure bending mode, but this is not so for composite Goland wing. The existence of the material coupling is the main reason for the coupling between the bending and torsional deformation in the four first modes. Figure 6.11 also shows that higher mode shapes of composite wing are more complex compared to wings made of isotropic material. This also could be attributed to both material and geometrical coupling.

6.2.3 Dynamics Response

In this section the effect of the material coupling on the dynamic response of composite Goland wing is mainly discussed. A number of selected cases with different material coupling coefficient K under a range of Mach numbers and velocities are investigated. As in the previous section, all other material parameters are kept constant apart from the material coupling coefficient in order to isolate and pinpoint its effect.

Figure 6.12 compares the generalized coordinates corresponding to the first mode for both isotropic and composite wing with $K = 15MN.m^2$ at Mach 0.75

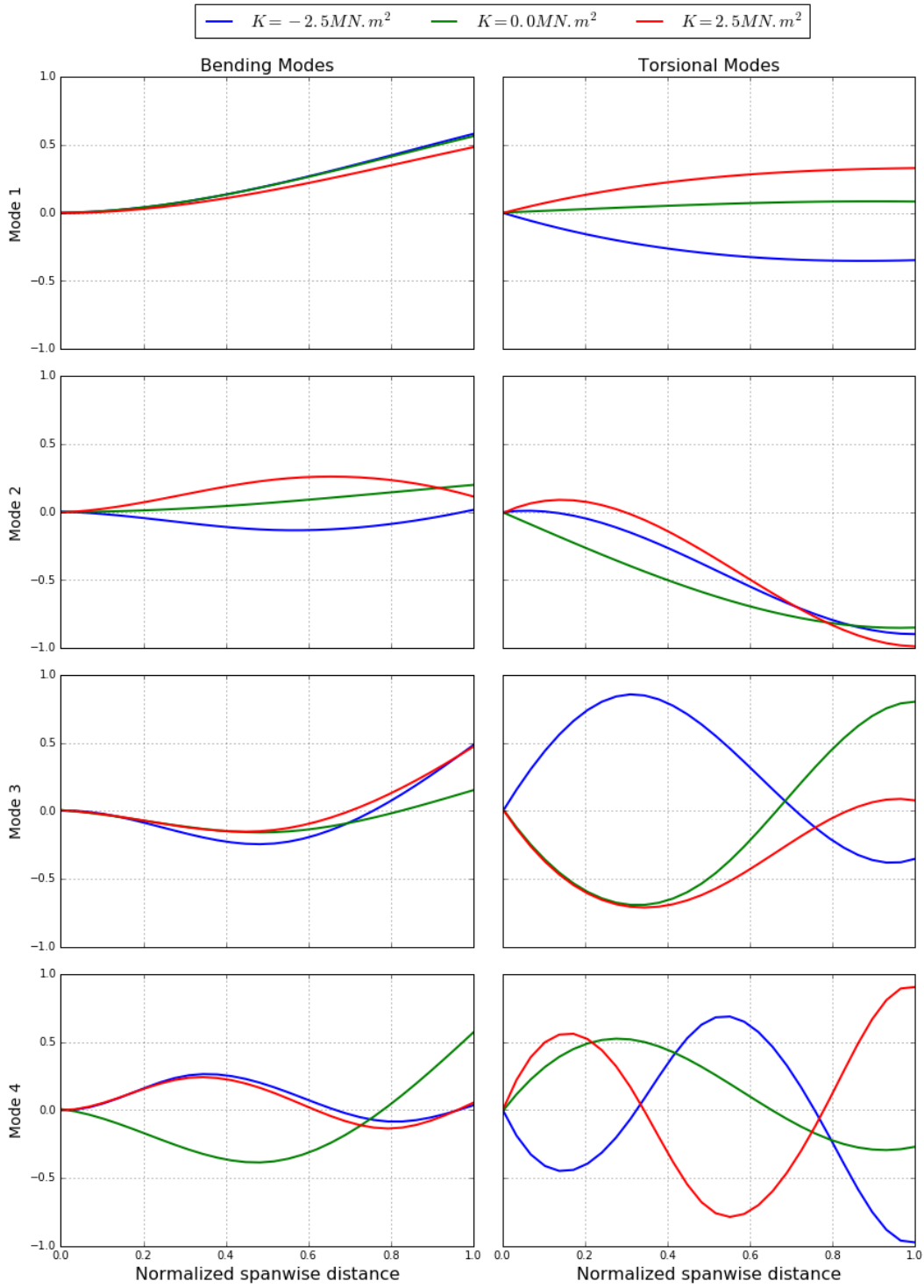

Figure 6.11: Mode shapes of composite Goland wing.

and velocity $110m/s$. This case shows a very slow damping response but it should be noted that it focuses on a small time window. It is clear that the amplitude of modal displacement is almost 50% less in the case of composite which reveals the advantage of using composites to reduce the vibration of the structure.

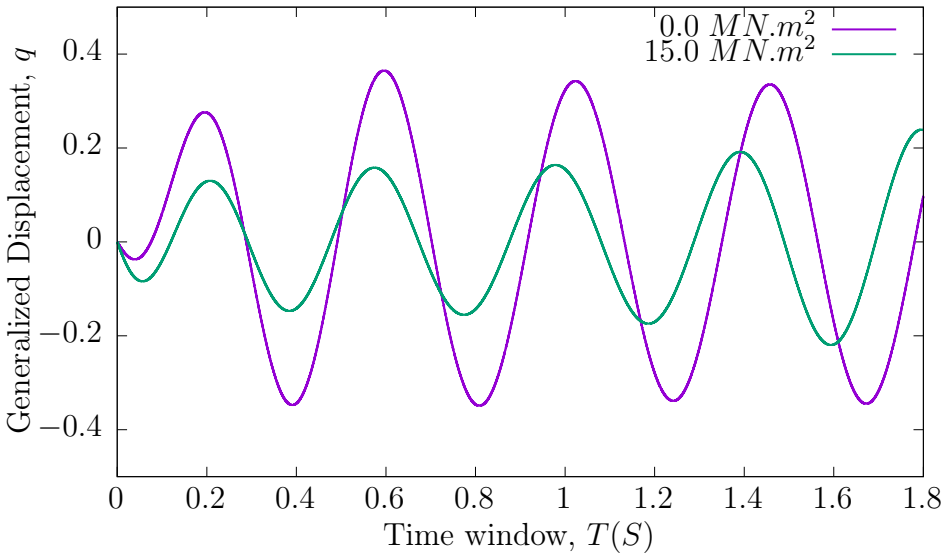

Figure 6.12: Near flutter point Response. $M_\infty = 0.75$, $V_\infty = 110m/s$.

Figure 6.13 shows another set of results for a subcritical speed at Mach 0.8 with three different material coupling values. Again, it is clear that the material coupling reduces the amplitude of the oscillation considerably. However, it also shows that the oscillation amplitude for $K = 15.0\ MN.m^2$ suggests that the damping is not always proportional to K values. It is worth mentioning here that the negative K values cases always diverge and therefore, they are not plotted here. These findings agree with Weisshaar and Ryan's theoretical analysis for rectangular wings [116].

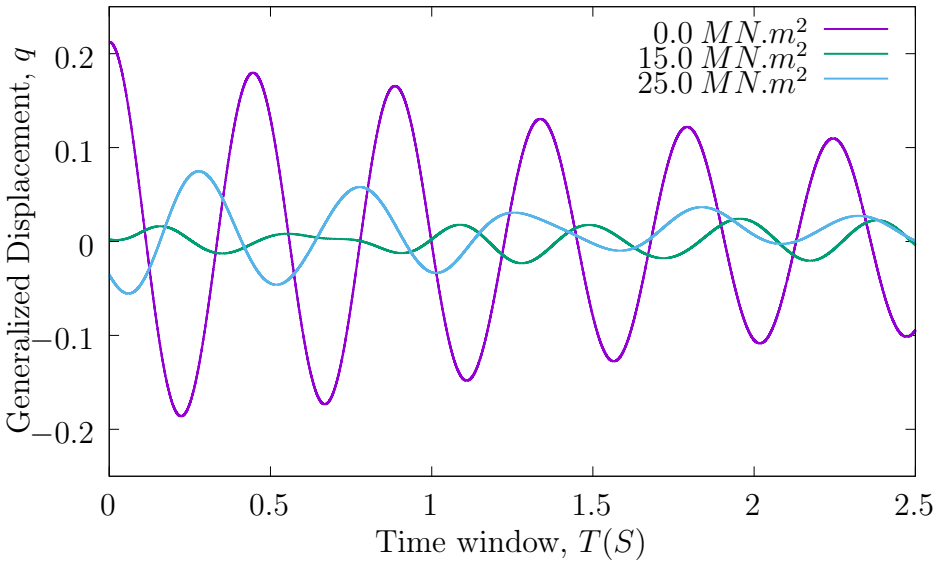

Figure 6.13: Near flutter point Response. $M_\infty = 0.80$, $V_\infty = 100m/s$.

6.3 Summary

This chapter represents three main validation steps of the newly developed model. It starts with a validation case of a rigid pitching wing in transonic flow. The predicted aerodynamics force and moment were compared against different codes from the literature which showed excellent agreement. Second step is on studying the free vibration behaviour of isotropic wing as well as its dynamics response. Again, the predicted results were compared and contrasted with previous studies. Finally, the material coupling effect on the dynamic response of composite wing was investigated. This chapter shows clearly the capabilities of this model and verifies the correctness of the developed code.

Chapter 7

Conclusions and Future Work

In addition to the summary at the end of each chapter, here the summary of principal final conclusions of the thesis given. The focus is on two main aspects, the significance of results and the overall methodology developed. This chapter ends by general recommendations and possible future directions based on the current work.

7.1 Principal Conclusions

Pertaining to the multi-aspect nature of the problem, this work has contributed to aeroelastic analysis particularly from a computational point of view. The main objective has been achieved, which was set out to predict the transonic flutter of composite wings, using the dynamic stiffness method coupled with high fidelity computational fluid dynamics model. The dynamic stiffness method has proven again tremendously advantageous as an indispensable tool for modal analysis. The model accuracy and efficiency are the core es-

sential attributes of this method. Moreover, the investigation has shown that DSM's elegant formulation can be implemented within modern CFD programming paradigm. This is a significant step towards implementing the method in modern structural dynamics and CFD software packages. Although DSM was primarily developed for frequency domain analysis, this work has successfully utilised it in the time domain. In general, this research has shown through different case studies the importance of considering the flow non-linearity when predicting the transonic flutter.

Considering how the aeroelastic problem has different aspects, such as aerodynamics, structural dynamics and coupling between them, it is therefore necessary to isolate each aspect of the problem first, towards establishing a thorough investigation. The nature of this problem has been reflected clearly in this work, when it began by investigating the free vibration characteristics of four different aircraft wings. These aircraft are within the categories of sailplanes and transport airliners, which have some common properties such as the high aspect ratios. On the other hand, they have some major differences too, in terms of the total mass, effects of engine weights , amongst others. These differences have been captured by the free vibration analysis of these aircraft.

The second main landmark in this study is the validation of the results within the aerodynamic framework by studying flow over two pitching airfoils, namely NACA0012 and NACA64A010 under different transonic conditions. These forced vibration cases exhibit interesting features leading to the understanding of aeroelastic problems. The results showed excellent agreement

with measured and modelled CFD investigations from the literature. More importantly, they proved the capability of Euler solvers in OpenFOAM and the dynamic mesh functionality. This particular phase of research ended by studying a typical two degrees of freedom airfoil model in transonic flow. It showed promising results which led to the next phase of the research, focusing on a complete aircraft elastic wing.

Following the same strategy, the last phase of this research started by validating the aerodynamics model of pitching Goland wing in transonic flow. The predicted aerodynamic forces showed a satisfactory agreement with numerical data published in the literature. Then the attention was confined to investigate the free vibration characteristics and aeroelastic behaviour of metallic Goland wing. The geometrical coupling effect was evident in the computed mode shapes. The flutter boundary of this case was predicted by the developed methodology and compared against different theories from the literature. A good agreement between similar theories was observed and also a sharp contrast between linear and non-linear theories was evident. Finally, a composite version of Goland wing was studied from structural dynamics point of view as well as from aeroelastic point of view. The significant differences between the free vibration modes of the composite wing and its metallic counterpart were demonstrated. Without doubt, the material coupling effect influenced the mode coupling in a major way, resulting in complex mode shapes. Additionally, the variation of material coupling on the aeroelastic properties was investigated, which showed its considerable influence on the oscillation characteristics. The main contribution made in this thesis is the prediction of

aeroelastic behaviour of metallic and composite wings in the transonic flow region by Euler-based CFD code OpenFOAM and the dynamic stiffness method.

7.2 Recommendations and Future Work

During this study the general framework for aeroelastic analysis has been developed and implemented successfully, which can be considered as a starting point in many future studies. Given the multidisciplinary nature of the problem, it will inspire future work in multiple directions. One possible direction is to include the structural damping effect on the aeroelatic characteristics of composite wings. This could lead to less conservative flutter boundary, yet it could increase the non-linearity of the system as well. Also, higher order structural theories and different element types could be used. For example, the beam theory could be extended to include the cross-sectional deformation, which could be a numerically efficient way to include the surface deformation. Different structural element types such as plates and shells could be incorporated and compared against the beam model. This will have applications for low aspect-ratio and delta wings. Appendix A provides some insights into the potential of such applications. A very significant development would be to extend the methodology to study complete aircraft configuration, which will require major development on both structural side as well as the aerodynamic side with advanced coupling algorithms.

From an aerodynamic point of view, the viscous effect could be studied by using Navier-Stokes solver which the current work-flow can handle with

minimal code development. However, as discussed before, such modes are still considered computationally expensive compared to Eular solver for aeroelastic analysis. Coupling optimization algorithms with the developed framework of this study could be also considered a significant contribution to select the wing material efficiently. Another very important feature would be to use the current framework to develop reduced order models, which could help minimise the computational time significantly. Furthermore, industrial applications would essentially benefit from incorporating a reduced order model with optimization algorithms. Of course, all of the above approaches are just limited number of the potential future developments in aeroelasticity based on the dynamic stiffness method.

Appendix A

Implementation in OpenFOAM

Considerable efforts were expended in developing the computer programs required in the investigation and this appendix gives a general description of the newly developed features and discusses its implementation into the methodology described in Chapter 3. As mentioned before the implementation is accomplished within the framework of OpenFOAM which is basically a C++ code. Due to the multi aspects nature of the problem formulation, such as equations of motion solver, fluid structure coupling, mesh deformation and many more other elements, it was necessary to design a modular code which decomposes these parts into smaller pieces. Therefore, this final code is designed as a library which consists of a number of C++ classes.

Figure A.1 shows the final structure of the code which has been developed and used in this thesis. The main concept is based on the fact that, in order to deform the wing in a particular mode, a special boundary condition is needed. This boundary condition deforms the fluid solver mesh at each time step based on the structural deformation. This newly developed boundary condition is

called `elasticBodyDisplacement`, which is the main user interface where the structure solver parameters in selected as in Listing A.1. This boundary condition is responsible for the communications between the `elasticBodyMotion` and the `elasticBodyForce` which are described in the next sections.

Figure A.1: Implemented code tree in OpenFOAM

A.1 elasticBodyDynamics

The user inputs in Figure A.1 will be described within the scope of each class shown in Figure A.1. Starting from the `elasticBodyDynamics` library which consists of few classes of subdivisions which constitute the core of this implementation. The `elasticBody` is a class which represents the structure as set of free vibration modes and discrete nodes. Every instance of this class reads the structure `type` (only beam type used in this study but the code

is ready to handle plates), the number of modes `nModes` and degrees of freedom of each node `nDof`. The implementation is fairly general and therefore, each node can have up to six degrees of freedom whose directions are specified through `transverse` direction and `rotation`. In the example showed in Listing A.1, the strucure has four natural modes and two degrees of freedom (transverse in the y direction and rotation about the z axis). Finally, the `Modes` and `Frequencies` entries are the file names where the mass normalised mode shapes and frequencies are stored.

```
wing
{
        type            elasticBodyDisplacement;
        value           uniform (0 0 0);
        structure
        {
                patch                   wing;
                type                    beam; //plate
                nModes                  4;
                nDof                    2;
                transverse              (0 1 0);
                rotation                (0 0 1);
                Modes                   (ModalMatrixH ModalMatrixP);
                Frequencies             Frequencies;
                odeSolver               RKCK45;
                // X Y Z thX thY thZ
                initialDisplacement  (0.0 0.0 0.0 0.0 0.0 0.0);
                initialVelocity      (0.0 0.0 0.0 0.0 0.0 -0.3);
                freeVib                 false;
        }

        mesh
        {
                corners     ((0 0 0) (6.1 0 0) (6.1 1.83 0) (0 1.83 0));
                nodesX1     10;
                nodesX2     1;
                orientation ZX;
        }

        forcesDict
        {
                type                elasticBodyMesh;
                patches             (wing);
                pName               p;
                UName               U;
                rhoName             rho;
                CofR                (0.6096 0 0.3048);
                pitchAxis           (0 0 1);
        }

}
```

Figure A.1: User input settings

Another important class is `elasticBodyMesh` which is a data member in `elasticBody` class. It defines the interpolation mesh which is essential for the fluid-structure coupling. This class locates the CFD mesh cells which are associated with each structure element. It requires four points which represents the mesh `corners`, number of nodes in each direction `nodesX1` and `nodesX2` and the `orientation` with respect to the coordinate axes. Also, this class was designed with plate element in mind and therefore, it has many features which is needed for plate surface deformation. The final part of Listing A.1 is required for the `elasticBodyForce` class which calculate the distributed force and moment over the `elasticBodyMesh`. It follows OpenFOAM original forces classes, therefore a full description of these inputs can be found in OpenFOAM user guide [117].

A.2 The library elasticBodyMotion

The second part of the implementation concerns the `elasticBodyMotion` library where most of the calculations are performed. In order to make the future development easier, the equation of motion is implemented in a separate class called `CSDODE` and its input is processed in a separate class called `CSDInput`. The only additional input for this class needed by the user is the ordinary differential equation solver called `odeSolver`. The `elasticBodyMotion` itself contains `elasticBody` which encapsulates all the needed information for the structure solver. For every time step, the `solveMotion` method calculates the displacement based on the time instance and distributed loads. The com-

puted generalized displacements are stored in `elasticBodyMotionState` class object, which is essential for parallel computing and restarting the simulation as required. In addition, it is referenced in `elasticBodyMotionFile` class for writing the required outputs such as displacements and modal coefficients.

A.3 Final Remarks

Despite the fact that the code developed for the thesis is not based on the first version, but has been refactored and iterated many times during the investigation. Naturally there is still a considerable scope for improvement and future developments. It could be generalised based on more abstract classes, for example a structural element abstract base class which can be reimplemented into concrete classes for beam and plate element separately. Also, for plates and shells considering their surface deformation, more complex interpolation techniques may be implemented. It is recommended that future developers should isolate the interpolation techniques in separate objects to simplify the interface for further future developments and to implement new mesh classes for complex structure geometries. Finally, the code could be further developed to include multiple elastic structures which could be used to model complete aircraft configuration.

Appendix B

Modal Analysis Code in Python

This appendix sheds some light on the implemented code in Python which has been developed and used in this thesis. The main objective of this code is to compute the mass normalized free vibration natural modes which are used as input for the solver, as described in Appendix A. For this development, again an object oriented programming concept has been used for the first time to implement the dynamic stiffness method which paves the way for more general and abstract implementations in future. In comparison with the development discussed in Appendix A, this code is relatively smaller (around 2000 lines of instructions compared to 5000 lines).

The general framework of the Python code is shown in Figure B.1 which consists of two main parts, namely core libraries (`src`) and executable applications (`APP`). Because Python is an interpreted language, the user can modify the script or create a new one and run it directly. So, these applications are merely examples, but the user can build as many executables as needed.

B.1 Material Properties

The first building block in the core library (`src`) is the material properties and how they are calculated. The most fundamental and base class is `laminatePly` which presents only one layer of material (ply). This class reads as input the ply orientation, ply thickness and the material properties and it is core function is computing the transformed Stiffness matrix. A list of `laminatePly` in the staking sequence then can be used as input for creating a composite `laminate`. This implementation allows each layer to have different ply angle, thickness and even material properties. Obviously, the main outcome of `laminate` is stiffness properties of the composite laminate. By taking a list of four `laminate` objects in addition to the dimensions of the beam box, the properties of composite boxed beam can be represented and computed by `beamBox` class. Due to the generality of the code any four `laminate` can be used. It is not necessary for the laminate to be similar or have the same material properties. However, it worth mentioning here that the two most common cases, namely CUS and CAS have be implemented a special cases to simplicity.

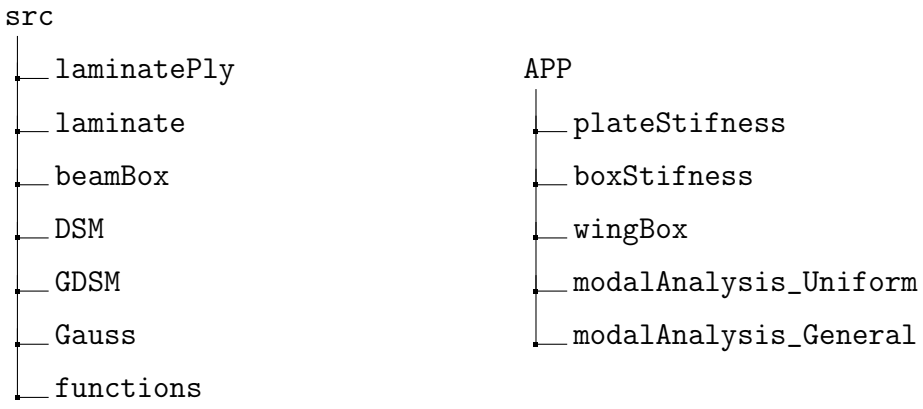

Figure B.1: Implemented code tree in Python

B.2 Modal Analysis

Three main classes have been developed in order to compute the free vibration modes based on the dynamic stiffness method. These are `DSM`, `GDSM` and `Gauss`. The `DSM` represents one composite beam element as describe in Section . This class can be reimplemented for any type of beam as needed without breaking the code dependency as long as the interface is kept the same. On the other hand, `GDSM` is the global dynamic stiffness matrix where all beam elements are assembled. It includes the Wittrick-Williams algorithm which uses standard Gauss elimination method which is implemented in `Gauss` class. The `Gauss` class is counting the negative elements along the diagonal after performing Gauss elimination. `GDSM` class search for the natural modes using the bisection method and normalise them if required.

B.3 Applications

With help of the `functions`, a few essential applications have been developed. As the names suggest, `plateStifness` and `boxStifness` are simple applications to calculate the material properties of composite plate and beam box respectively. By contrast, `wingBox` is for non-uniform wings which consists of varying wing boxes along the wing span. The output from this program can be used later for modal analysis of non-uniform wings. For modal analysis, there are two applications one for uniform beam and one for non-uniform, namely `modalAnalysis_Uniform` and `modalAnalysis_General`. Both are able to produce mass normalised mode shapes and can plot the mode shapes

automatically if needed. On the contrary, `modalAnalysis_General` reads the input from `CSV` file which is convenient and can be created with MS-Excel or any text editor.

B.4 Final Remarks

As mentioned in Appendix A, there is a wide scope for code improvement. Despite the fact that Python is not as advanced as C++ in terms of high level object oriented concepts, the code can be more generalized. Future improvement could be achieved by taking advantage of parallel computing to speed-up the calculations. Also, more efficient implementation of the bisection method could increase the speed considerably. Additionally, different beam types and plates could be implemented as well. A major development could be to include double cells beam box and curved boxes. Finally, more applications could be utilised to meet the user needs.

Bibliography

[1] J. R. Banerjee, X. Liu, H. Kassem, "Free vibration and flutter characteristics of high aspect ratio aircraft wings", *12th Conference Dynamical Systems - Theory and Applications*, Dynamical Systems - Theory and Applications, 2013, pp. 15–26.

[2] J. R. Banerjee, X. Liu, H. I. Kassem, "Aeroelastic stability analysis of high aspect ratio aircraft wings", *Journal of Applied Nonlinear Dynamics*, 3, 4, 2014, pp. 413–422.

[3] H. I. Kassem, X. Liu, J. R. Banerjee, "Flutter Analysis using a Fully Coupled Density Based Solver for Inviscid Flow", *Proceedings of The Twelfth International Conference on Computational Structures Technology*, ed. by B. H. V. Topping, I. P, Paper 146, Civil-Comp Press, Stirlingshire, UK, 2014.

[4] H. I. Kassem, J. R. Banerjee, "Transonic Speed Flutter Analysis of a Rectangular Wing using the OpenFOAM Computational Fluid Dynamics Code and the Dynamic Stiffness Method", *The Fifteenth International Conference on Civil, Structural and Environmental Engineering Computing*, ed. by J. Kruis, Y. Tsompanakis, B. H. V. Topping, Paper 110, Civil-Comp Press, Stirlingshire, UK, 2015.

[5] H. I. Kassem, X. Liu, J. R. Banerjee, "Transonic flutter analysis using a fully coupled density based solver for inviscid flow", *Advances in Engineering Software*, 95, 2016, pp. 1–6.

[6] B. Harris, *Engineering composite materials*, Publications of the Institute of Materials, Minerals and Mining, Maney Publishing, 1999.

[7] A. Lucas, J. Harris, *Ancient Egyptian Materials and Industries*, Courier Corporation, 2012.

[8] P. T. Nicholson, I. Shaw, *Ancient Egyptian Materials and Technology*, Cambridge University Press, 2000.

[9] D. P. Raymer, *Aircraft design: a conceptual approach*, American Institute of Aeronautics and Astronautics, 1989.

[10] S. Dutton, D. Kelly, A. Baker, *Composite Materials for Aircraft Structures*, 2nd ed., AIAA Education Series, American Institute of Aeronautics and Astronautics, 2004.

[11] Hannes Ross, "Fly Around the World with a Solar Powered Airplane", *The 26th Congress of ICAS and 8th AIAA ATIO*, Aviation Technology, Integration, and Operations (ATIO) Conferences, Alaska: American Institute of Aeronautics and Astronautics, 2008.

[12] R. Laurenzo, "Soaring on a Solar Impulse", *Aerospace America*, 47, 5, 2009, pp. 32–36.

[13] R. Bisplinghoff, H. Ashley, R. Halfman, *Aeroelasticity*, Dover Books on Aeronautical Engineering Series, Dover Publications, 1996.

[14] Y. C. Fung, *An Introduction to the Theory of Aeroelasticity*, Dover Phoenix Edition: Engineering, Dover Publications, Incorporated, 2002.

[15] R. Clark, D. Cox, H. Curtiss, E. Dowell, J. Edwards, K. Hall, D. Peters, R. Scanlan, E. Simiu, F. Sisto, *A Modern Course in Aeroelasticity*, Solid Mechanics and Its Applications, Kluwer Academic Publishers, 2006.

[16] J. R. Banerjee, "The Dynamic Stiffness Method: Theory, Practice and Promise", *Computational Technology Reviews*, 11, 2015, pp. 31–57.

[17] K. Isogai, "On the Transonic-Dip Mechanism of Flutter of a Sweptback Wing", *AIAA Journal*, 17, 7, 1979, pp. 793–795.

[18] K. Isogai, "Transonic dip mechanism of flutter of a sweptback wing. II", *AIAA Journal*, 19, 9, 1981, pp. 1240–1242.

[19] O. O. Bendiksen, "Review of unsteady transonic aerodynamics: Theory and applications", *Progress in Aerospace Sciences*, 47, 2, 2011, pp. 135–167.

[20] R. M. Bennett, J. W. Edwards, "An overview of recent developments in computational aeroelasticity", *29th AIAA, Fluid Dynamics Conference, Fluid Dynamics and Co-located Conferences,* paper 2421, 1998.

[21] O. O. Bendiksen, G. Seber, "Fluid–structure interactions with both structural and fluid nonlinearities", *Journal of Sound and Vibration*, 315, 3, 2008, pp. 664–684.

[22] G. P. Guruswamy, "A review of numerical fluids/structures interface methods for computations using high-fidelity equations", *Computers & structures*, 80, 1, 2002, pp. 31–41.

[23] D. M. Schuster, D. D. Liu, L. J. Huttsell, "Computational aeroelasticity: success, progress, challenge", *Journal of Aircraft*, 40, 5, 2003, pp. 843–856.

[24] O. O. Bendiksen, "Modern developments in computational aeroelasticity", *Proceedings of the Institution of Mechanical Engineers, Part G: Journal of Aerospace Engineering*, 218, 3, 2004, pp. 157–177.

[25] G. Guruswamy, "Impact of parallel computing on high fidelity based multidisciplinary analysis", *7th AIAA/USAF/NASA/ISSMO Symposium on Multidisciplinary Analysis and Optimization*, Multidisciplinary Analysis Optimization Conferences, American Institute of Aeronautics and Astronautics, 1998.

[26] T. Theodorsen, *General Theory of Aerodynamic Instability and the Mechanism of Flutter*, Technical Report NACA-TR-496, NASA, 1949.

[27] M. Blair, *A Compilation of the Mathematics Leading to the Doublet Lattice Method*, Technical Report WL-TR-92-3028, Wright Laboratory, 1992.

[28] E. Livne, "Future of Airplane Aeroelasticity", *Journal of Aircraft*, 40, 6, 2003, pp. 1066–1092.

[29] J. D. Anderson, *Fundamentals of Aerodynamics*, 5th ed., McGraw-Hill, 2011.

[30] M. T. Landahl, M. Landahl, *Unsteady Transonic Flow*, Cambridge University Press, 1989.

[31] J. D. Cole, E. M. Murman, "Calculation of plane steady transonic flows", *AIAA Journal*, 9, 1, 1971, pp. 114–121.

[32] J. D. Cole, "Modern Developments in Transonic Flow", *SIAM Journal on Applied Mathematics*, 29, 4, 1975, pp. 763–787.

[33] D. Nixon, "Basic Equations for Unsteady Transonic Flow", *Unsteady Transonic Aerodynamics*, Progress in Astronautics and Aeronautics, American Institute of Aeronautics and Astronautics, 1989, pp. 57–73.

[34] W. Ballhaus, F. Bailey, "Numerical calculation of transonic flow about swept wings", *Society of Naval Architects and Marine Engineers, and U.S. Navy, Advanced Marine Vehicles Meeting*, Advanced Marine Vehicles Conferences, American Institute of Aeronautics and Astronautics, 1972.

[35] W. Mason, D. Mackenzie, M. Stern, J. Johnson, "A numerical three-dimensional viscous transonic wing-body analysis and design tool", *16th Aerospace Sciences Meeting*, American Institute of Aeronautics and Astronautics, 1978.

[36] C. Boppe, M. Stern, "Simulated transonic flows for aircraft with nacelles, pylons, and winglets", *18th Aerospace Sciences Meeting*, American Institute of Aeronautics and Astronautics, 1980.

[37] J. T. Batina, "Efficient algorithm for solution of the unsteady transonic small-disturbance equation", *Journal of Aircraft*, 25, 7, 1988, pp. 598–605.

[38] J. W. Edwards, "Transonic shock oscillations calculated with a new interactive boundary layer coupling method", *31st Aerospace Sciences Meeting*, American Institute of Aeronautics and Astronautics, 1993.

[39] J. W. Edwards, "Calculated viscous and scale effects on transonic aeroelasticity", 1998.

[40] J. W. Edwards, "Calculated Viscous and Scale Effects on Transonic Aeroelasticity", *Journal of Aircraft*, 45, 6, 2008, pp. 1863–1871.

[41] R. Magnus, H. Yoshihara, "Inviscid transonic flow over airfoils", *AIAA Journal*, 8, 12, 1970, pp. 2157–2162.

[42] R. Magnus, H. Yoshihara, "Unsteady Transonic Flows over an Airfoil", *AIAA Journal*, 13, 12, 1975, pp. 1622–1628.

[43] A. Jameson, T. Baker, N. Weatherill, "Calculation of Inviscid Transonic Flow over a Complete Aircraft", *24th Aerospace Sciences Meeting*, American Institute of Aeronautics and Astronautics, 1986.

[44] D. M. Schuster, J. Vadyak, E. Atta, *Flight loads prediction methods for fighter aircraft*, WRDC-TR-89-3104, November, 1989.

[45] M. Smith, D. Schuster, L. Huttsell, B. Buxton, "Development of an Euler/Navier-Stokes aeroelastic method for three-dimensional vehicles with multiple flexible surfaces", *37th Structure, Structural Dynamics and Materials Conference*, Structures, Structural Dynamics, and Materials and Co-located Conferences, American Institute of Aeronautics and Astronautics, 1996.

[46] D. M. Schuster, P. S. Beran, L. J. Huttsell, *Application of the ENS3DAE Euler/Navier-Stokes aeroelastic method*, AGARD Report 822, 1998.

[47] C. Borland, *XTRAN3S-Transonic Steady and Unsteady Aerodynamics for Aeroelastic Applications*, AFWAL-TR-85-3124, Air Force Wright Aeronantical Laboratories, 1986.

[48] S. Robert C, H. Sherwood T, W. Carol D, D. Michael H, "The Benchmark Active Controls Technology Model Aerodynamic Data", *Journal of Guidance, Control, and Dynamics*, 23, 5, 2000, pp. 914–921.

[49] A. P. Lewis, M. J. Smith, "Euler-Based Dynamic Aeroelastic Analysis of Shell Structures", *Journal of Aircraft*, 37, 5, 2000, pp. 840–845.

[50] W. Sutherland, "LII. The viscosity of gases and molecular force", *Philosophical Magazine*, 36, 223, 1893, pp. 507–531.

[51] D. C. Wilcox, *Turbulence modeling for CFD*, 2nd ed., DCW, 1998.

[52] S. Pope, *Turbulent Flows*, Cambridge University Press, 2000.

[53] P. Davidson, *Turbulence: An Introduction for Scientists and Engineers*, Oxford University Press, 2015.

[54] E. Lee-Rausch, J. T. Baitina, "Wing flutter computations using an aerodynamic model based on the Navier-Stokes equations", *Journal of Aircraft*, 33, 6, 1996, pp. 1139–1147.

[55] *CFL3D User's Manual (Version 5.0)*, NASA Langley Technical Report Server, 1998.

[56] R. E. Bartels, D. M. Schuster, "Comparison of Two Navier-Stokes Methods with Benchmark Active Control Technology Experiments", *Journal of Guidance, Control, and Dynamics*, 23, 6, 2000, pp. 1094–1099.

[57] L. Huttsell, D. Schuster, J. Volk, J. Giesing, M. Love, "Evaluation of computational aeroelasticity codes for loads and flutter", *39th Aerospace Sciences Meeting and Exhibit*, Aerospace Sciences Meetings, American Institute of Aeronautics and Astronautics, 2001.

[58] J. G. Marshall, M. Imregun, "A review of aeroelasticity methods with emphasis on turbomachinery applications", *Journal of Fluids and Structures*, 10, 3, 1996, pp. 237–267.

[59] V. Koloušek, "Anwendung des Gesetzes der virtuellen Verschiebungen und des Reziprozitätssatzes in der Stabwerksdynamik", *Ingenieur-Archiv*, 12, 6, 1941, pp. 363–370.

[60] V. Koloušek, "Berechnung der schwingenden Stockwerkrahmen nach der Deformationsmethode", *Der Stahlbau*, 16, 1943, pp. 5–6.

[61] F. Williams, W. Wittrick, "An automatic computational procedure for calculating natural frequencies of skeletal structures", *International Journal of Mechanical Sciences*, 12, 9, 1970, pp. 781–791.

[62] W. H. Wittrick, F. W. Williams, "A general algorithm for computing natural frequencies of elastic structures", *Quarterly Journal of Mechanics and Applied Mathematics*, 24, 3, 1971, pp. 263–284.

[63] F. W. Williams, W. H. Wittrick, "Efficient calculation of natural frequencies of certain marine structures", *International Journal of Mechanical Sciences*, 15, 10, 1973, pp. 833–843.

[64] F. Y. Cheng, W.-H. Tseng, "Dynamic matrix of Timoshenko beam columns", *Journal of the Structural Division*, 99, 3, 1973, pp. 527–549.

[65] W. P. Howson, F. W. Williams, "Natural frequencies of frames with axially loaded Timoshenko Members", *Journal of Sound and Vibration*, 26, 4, 1973, pp. 503–515.

[66] B. A. Akesson, "PFVIBAT: a computer program for plane frame vibration analysis by an exact method", *International Journal for Numerical Methods in Engineering*, 10, 6, 1976, pp. 1221–1231.

[67] F. W. Williams, W. P. Howson, "Compact computation of natural frequencies and buckling loads for plane frames", *International Journal for Numerical Methods in Engineering*, 11, 7, 1977, pp. 1067–1081.

[68] M. Anderson, F. W. Williams, J. R. Banerjee, B. J. Durling, C. L. Herstrom, D. Kennedy, D. B. Warnaar, *User manual for BUNVIS-RG: an exact buckling and vibration program for lattice structures, with repetitive geometry and substructuring options*, Technical Report NASA-TM-87669, NASA, 1986.

[69] J. R. Banerjee, F. W. Williams, "Exact Bernoulli–Euler dynamic stiffness matrix for a range of tapered beams", *International Journal for Numerical Methods in Engineering*, 21, 1985, pp. 2289–2302.

[70] J. R. Banerjee, F. W. Williams, "Exact Bernoulli-Euler static stiffness matrix for a range of tapered beam-columns", *International Journal for Numerical Methods in Engineering*, 23, 1986, pp. 1615–1628.

[71] W. L. Hallauer Jr., R. Y. L. Liu, "Beam bending-torsion dynamic stiffness method for calculation of exact vibration modes", *Journal of Sound and Vibration*, 85, 1, 1982, pp. 105–113.

[72] P. O. Friberg, "Coupled vibrations of beams - an exact dynamic element stiffness matrix", *International Journal for Numerical Methods in Engineering*, 19, 4, 1983, pp. 479–493.

[73] J. R. Banerjee, "Coupled bending–torsional dynamic stiffness matrix for beam elements", *International Journal for Numerical Methods in Engineering*, 28, 3, 1989, pp. 1283–1298.

[74] J. R. Banerjee, "A FORTRAN routine for computation of coupled bending-torsional dynamic stiffness matrix of beam elements", *Advances in Engineering Software and Workstations*, 13, 1, 1991, pp. 17–24.

[75] J. R. Banerjee, "Development of an exact dynamic stiffness matrix for free vibration analysis of a twisted Timoshenko beam", *Journal of Sound and Vibration*, 270, 1, 2004, pp. 379–401.

[76] J. R. Banerjee, H. Su, "Development of a dynamic stiffness matrix for free vibration analysis of spinning beams", *Computers & Structures*, 82, 23, 2004, pp. 2189–2197.

[77] A. Pagani, M. Boscolo, J. Banerjee, E. Carrera, "Exact dynamic stiffness elements based on one-dimensional higher-order theories for free vibration analysis of solid and thin-walled structures", *Journal of Sound and Vibration*, 332, 23, 2013, pp. 6104–6127.

[78] F. W. Williams, J. R. Banerjee, "Free vibration of composite beams-an exact method using symbolic computation", *Journal of Aircraft*, 32, 3, 1995, pp. 636–642.

[79] J. R. Banerjee, "Free vibration of axially loaded composite Timoshenko beams using the dynamic stiffness matrix method", *Computers & structures*, 69, 2, 1998, pp. 197–208.

[80] M. Eisenberger, H. Abramovich, O. Shulepov, "Dynamic stiffness analysis of laminated beams using a first order shear deformation theory", *Composite Structures*, 31, 4, 1995, pp. 265–271.

[81] J. R. Banerjee, H. Su, C. Jayatunga, "A dynamic stiffness element for free vibration analysis of composite beams and its application to aircraft wings", *Computers & Structures*, 86, 6, 2008, pp. 573–579.

[82] M. Smith, C. Cesnik, D. Hodges, K. Moran, "An evaluation of computational algorithms to interface between CFD and CSD methodologies", *37th Structure, Structural Dynamics and Materials Conference*, Structures, Structural Dynamics, and Materials and Co-located Conferences, American Institute of Aeronautics and Astronautics, 1996.

[83] P. Girodroux-Lavigne, J. P. Grisval, S. Guillemot, M. Henshaw, A. Karlsson, V. Selmin, J. Smith, E. Teupootahiti, B. Winzell, "Comparison of static and dynamic fluid-structure interaction solutions in the case of a highly flexible modern transport aircraft wing", *Aerospace Science and Technology*, 7, 2, 2003, pp. 121–133.

[84] P. Guruswamy, T. Yang, "Aeroelastic time response analysis of thin airfoils by transonic code LTRAN2", *Computers & Fluids*, 9, 4, 1981, pp. 409–425.

[85] J. H. Ferziger, M. Perić, *Computational methods for fluid dynamics*, 3rd ed., Springer Berlin, 1996.

[86] H. K. Versteeg, W. Malalasekera, *An Introduction to Computational Fluid Dynamics: The Finite Volume Method*, 2nd ed., Pearson Education Limited, 2007.

[87] C. J. Greenshields, H. G. Weller, L. Gasparini, J. M. Reese, "Implementation of semi-discrete, non-staggered central schemes in a colocated, polyhedral, finite volume framework, for high-speed viscous flows", *International journal for numerical methods in fluids*, 63, 1, 2010, pp. 1–21.

[88] L. F. G. Marcantoni, J. P. Tamagno, S. A. Elaskar, "High Speed Flow Simulation Using OpenFOAM", *Mecánica Computacional Vol XXXI*, Asociación Argentina de Mecánica Computacional, 2012, pp. 2936–2959.

[89] A. Kurganov, E. Tadmor, "New High-Resolution Central Schemes for Nonlinear Conservation Laws and Convection–Diffusion Equations", *Journal of Computational Physics*, 160, 1, 2000, pp. 241–282.

[90] H. Jasak, Z. Tukovic, "Automatic mesh motion for the unstructured finite volume method", *Transactions of FAMENA*, 30, 2, 2006, pp. 1–20.

[91] H. Jasak, "Dynamic Mesh Handling in OpenFOAM", *43rd AIAA Aerospace Sciences Meeting and Exhibit*, 2008, pp. 1–10.

[92] H. Jasak, A. Jemcov, Z. Tukovic, "OpenFOAM: A C++ library for complex physics simulations", *International Workshop on Coupled Methods in Numerical Dynamics, IUC, Dubrovnik, Croatia*, 2007, pp. 1–20.

[93] D. Givoli, "Non-reflecting boundary conditions", *Journal of Computational Physics*, 94, 1, 1991, pp. 1–29.

[94] W. Rodden, *Theoretical and Computational Aeroelasticity*, Crest Publishing, 2011.

[95] J. Alonso, A. Jameson, "Fully-implicit time-marching aeroelastic solutions", *32nd Aerospace Sciences Meeting and Exhibit*, American Institute of Aeronautics and Astronautics, 1994.

[96] F. Liu, J. Cai, Y. Zhu, H. M. Tsai, A. S. F. Wong, "Calculation of Wing Flutter by a Coupled Fluid-Structure Method", *Journal of Aircraft*, 38, 2, 2001, pp. 334–342.

[97] R. Kamakoti, Y. Lian, S. Regisford, A. Kurdila, W. Shyy, "Computational aeroelasticity using a pressure-based solver", *CMES- Computer Modeling in Engineering and Sciences*, 3, 6, 2002, pp. 773–789.

[98] J. R. Banerjee, "Dynamic stiffness formulation for structural elements: a general approach", *Computers & structures*, 63, 1, 1997, pp. 101–103.

[99] A. Y. T. Leung, *Dynamic Stiffness and Substructures*, Springer, London, 1993.

[100] G. P. Guruswamy, "Ensaero: A multidisciplinary program for fluid/structural interaction studies of aerospace vehicles", *Computing Systems in Engineering*, Computational Technology for Flight Vehicles, 1, 2, 1990, pp. 237–256.

[101] H. Weller, G. Tabor, H. Jasak, C. Fureby, "A tensorial approach to computational continuum mechanics using object-oriented techniques", *Computers in Physics*, 12, 6, 1998, pp. 620–631.

[102] S. Yang, S. Luo, F. Liu, H.-M. Tsai, "Subsonic flow over unstalled pitching airfoil computed by Euler method", *AIAA Fluid Dynamics Conference and Exhibit*, 2006, pp. 1–16.

[103] W. McCroskey, S. Puccif, "Viscous-inviscid interaction on oscillating airfoils in subsonic flow", *AIAA Journal*, 20, 2, 1982, pp. 167–174.

[104] S. S. Davis, "NACA 64A010 (NASA Ames Model) oscillatory pitching", *AGARD Report*, 702, 1982.

[105] X. Chen, G. Zha, Z. Hu, M. T. Yang, "Flutter Prediction Based on Fully Coupled Fluid-Structural Interactions", *9th National Turbine Engine High Cycle Fatigue Conference*, 2004.

[106] C. Geuzaine, J. F. Remacle, "Gmsh: A 3-D finite element mesh generator with built-in pre-and post-processing facilities", *International Journal for Numerical Methods in Engineering*, 79, 11, 2009, pp. 1309–1331.

[107] M. McMullen, A. Jameson, J. Alonso, "Application of a non-linear frequency domain solver to the Euler and Navier-Stokes equations", *AIAA paper*, 120, 2002.

[108] J. R. Cash, A. H. Karp, "A variable order Runge-Kutta method for initial value problems with rapidly varying right-hand sides", *ACM Transactions on Mathematical Software (TOMS)*, 16, 3, 1990, pp. 201–222.

[109] F. E. Eastep, J. Olsen, "Transonic Flutter Analysis of a Rectangular Wing with Conventional Airfoil Sections", *AIAA Journal*, 18, 10, 1980, pp. 1159–1164.

[110] G. H. Parker, "Dynamic Aeroelastic Analysis of Wing/Store Configurations", PhD thesis, Air Force Institute of Technology, 2005.

[111] P. S. Beran, N. S. Khot, F. E. Eastep, R. D. Snyder, J. V. Zweber, *The Dependence of Store-Induced Limit-Cycle Oscillation Predictions on Modelling Fidelity*, ADP014183, Multidisciplinary Technologies Center Air Force Research Laboratory (AFRL), 2003.

[112] P. S. Beran, T. W. Strganac, K. Kim, C. Nichkawde, "Studies of Store-Induced Limit-Cycle Oscillations Using a Model with Full System Nonlinearities", *Nonlinear Dynamics*, 37, 4, 2004, pp. 323–339.

[113] M. Kurdi, N. Lindsley, P. Beran, "Uncertainty quantification of the Goland wing's flutter boundary", *AIAA Atmospheric Flight Mechanics Conference and Exhibit*, AIAA, 2007, pp. 20–23.

[114] M. Goland, "The flutter of a uniform cantilever wing", *Journal of Applied Mechanics-Transactions of the Asme*, 12, 4, 1945, A197–A208.

[115] C. Chung, S. Shin, "Worst case flutter analysis of a stored wing with structural and aerodynamic variation", *AIAA Structures, Structural Dynamics, and Materials Conference, Orlando, Florida.* 2010.

[116] T. A. Weisshaar, R. J. Ryan, "Control of aeroelastic instabilities through stiffness cross-coupling", *Journal of Aircraft*, 23, 2, 1986, pp. 148–155.

[117] *OpenFOAM v2.3 User Guide*, 2014.